

This is an Accepted Manuscript for *Annals of Glaciology*. Subject to change during the editing and production process.

DOI: 10.1017/aog.2024.41

# Spatiotemporal mass balance variability of Jostedalsbreen ice cap, Norway, revealed by a temperature-index model with data assimilation

Kamilla Hauknes Sjursen<sup>1</sup>, Thorben Dunse<sup>1</sup>, Thomas Vikhamar Schuler<sup>2</sup>, Liss Marie Andreassen<sup>3</sup>,  
Henning Åkesson<sup>2</sup>

<sup>1</sup>*Department of Civil Engineering and Environmental Sciences, Western Norway University of Applied Sciences, Sogndal, Norway*

<sup>2</sup>*Department of Geosciences, University of Oslo, Oslo, Norway*

<sup>3</sup>*Norwegian Water Resources and Energy Directorate (NVE), Oslo, Norway*

*Correspondence: Kamilla Hauknes Sjursen <kamilla.hauknes.sjursen@hvl.no>*

**ABSTRACT.** Jostedalsbreen in western Norway is mainland Europe's largest ice cap and a complex system of more than 80 glaciers. While observational records indicate a significant sensitivity to climate fluctuations, knowledge about ice-cap wide spatiotemporal mass changes and their drivers remain sparse. Here, we quantify the surface mass balance (SMB) of Jostedalsbreen from 1960–2020 using a temperature-index model within a Bayesian framework. We assimilate seasonal glaciological SMB to constrain accumulation and ablation, and geodetic mass balance to adjust model parameters for each glacier individually. Overall, we find that Jostedalsbreen has experienced a small mass loss of  $-0.07$  m w.e.  $a^{-1}$  ( $-0.21$ – $0.08$  m w.e.  $a^{-1}$ ), but with substantial spatiotemporal variability. Our results suggest that winter SMB variations were the main control on annual SMB between 1960–2000, while increasingly negative summer SMB is responsible for substantial mass losses after 2000. Spatial variations in SMB between glaciers or regions of the ice cap are likely associated with local topography and its effect on orographic precipitation. We advocate for models to leverage the growing availability of observational resources to improve SMB predictions. We demonstrate an approach that

This is an Open Access article, distributed under the terms of the Creative Commons Attribution-NonCommercial-NoDerivatives licence (<http://creativecommons.org/licenses/by-nc-nd/4.0/>), which permits non-commercial re-use, distribution, and reproduction in any medium, provided the original work is unaltered and is properly cited. The written permission of Cambridge University Press must be obtained for commercial re-use or in order to create a derivative work.

28 **assimilates complementary datasets, while addressing their inherent uncer-**  
29 **tainties, to constrain models and provide robust estimates of spatiotemporal**  
30 **SMB and associated uncertainties.**

## 31 **1 INTRODUCTION**

32 Jostedalbreen ice cap is the largest glacier in mainland Europe and constitutes around 20% of the glacier-  
33 ized area in Norway (Andreassen and others, 2022). Situated in a sparsely populated area in western  
34 Norway, the ice cap is a major tourist attraction, stimulating local business and supporting livelihoods, in  
35 addition to providing meltwater runoff for hydropower production, agriculture and ecosystems. Jostedal-  
36 breen is a complex glacier system divided into more than 80 units (Andreassen and others, 2022), some of  
37 which have been monitored through glaciological, geodetic or front position surveys over shorter or longer  
38 time periods during the past century (e.g. Winkler, 1996; Andreassen and others, 2020, 2023; Kjøllmoen  
39 and others, 2022).

40 Owing to the maritime climate in the region, with relatively mild summers and precipitation-rich  
41 winters, glaciers of Jostedalbreen experience substantial mass-turnover and are sensitive to climate fluctu-  
42 ations (Oerlemans, 1992; Nesje and others, 2000; Winkler and others, 2009). The most notable example is  
43 a period of mass gain during the 1990s, documented in the long-term glaciological mass-balance records of  
44 Nigardsbreen and Austdalsbreen, and the subsequent advances of several outlet glaciers (e.g. Andreassen  
45 and others, 2005, 2020; Winkler and others, 2009; Kjøllmoen and others, 2022). Since the early 2000s,  
46 glaciological mass balance, derived from interpolation of stake measurements on the glacier surface, and  
47 front position measurements indicate significant mass loss and retreat, although years with mass surplus  
48 are still registered, e.g. 2012, 2020 (Andreassen and others, 2020; Kjøllmoen and others, 2022).

49 Current and future climate change is expected to accelerate glacier mass loss and retreat, which in  
50 turn may alter runoff regimes of glacierized catchments in Norway (e.g. Nesje and others, 2008; Giesen and  
51 Oerlemans, 2010; Engelhardt and others, 2015; Hanssen-Bauer and others, 2017; Compagno and others,  
52 2021; Nesje, 2023). Future retreat of major outlet glaciers of Jostedalbreen or complete disintegration of  
53 the ice cap would have strong ecological and economic implications in the region, and could increase the  
54 risk of glacier and/or paraglacial hazards (Jackson and Ragulina, 2014; Haeberli and Whiteman, 2021).  
55 Understanding the response of glaciers and ice caps to climate change requires knowledge about mass

56 changes in space and time. For Jostedalbreen, mass changes from existing observational records are difficult  
57 to reconcile, as these only provide temporal and spatial snapshots. For example, long-term glaciological  
58 mass-balance records only exist for two glaciers (Nigardsbreen and Austdalsbreen; Kjølmoen and others,  
59 2022), and meaningful geodetic mass-balance estimates are available only at multi-year intervals (e.g.  
60 Hugonnet and others, 2021; Andreassen and others, 2023) and with incomplete spatial coverage (Andreassen  
61 and others, 2020, 2023). Modelling studies on Jostedalbreen are also limited to selected outlet glaciers (e.g.  
62 Oerlemans, 1997; Laumann and Nesje, 2009; Engelhardt and others, 2014; Li and others, 2015; Trachsel  
63 and Nesje, 2015; Sjursen and others, 2023).

64 Glacier mass-balance models are valuable tools to investigate glacier mass changes and provide SMB  
65 estimates with complete temporal and spatial coverage. Common modelling approaches range from physics-  
66 based energy-balance approaches (e.g. Andreassen and Oerlemans, 2009; Giesen and Oerlemans, 2010;  
67 Zolles and others, 2019; Eidhammer and others, 2021) to relatively simple temperature-index models (e.g.  
68 Schuler and others, 2005; Engelhardt and others, 2014; Huss and Hock, 2015; Geck and others, 2021) that  
69 parameterize the relationship between temperature and melt (see e.g. Hock, 2005; Zekollari and others,  
70 2022). While energy-balance models provide complete representation of the underlying physical processes,  
71 they often suffer from a lack of detailed in-situ meteorological data and coarse-resolution climate model data  
72 (Réveillet and others, 2018). Therefore, simpler, less input-demanding temperature-index models are often  
73 preferred, as they only require temperature and precipitation as meteorological input, both of which are  
74 more readily available in many areas of the world. However, the performance of temperature-index models  
75 heavily depends on model parameter values and their calibration to site-specific mass-balance observations  
76 (Schuster and others, 2023).

77 In-situ observations of glacier mass change, e.g. through the glaciological method, are sparse and  
78 concentrated to a handful of well-monitored regions (WGMS, 2024). This challenge is only recently starting  
79 to become alleviated by increased spatial coverage of geodetic mass balance derived from satellite-sensed  
80 surface elevation changes (e.g. Dussaillant and others, 2019; Shean and others, 2020; Hugonnet and others,  
81 2021). Consequently, satellite-borne geodetic mass balances are increasingly used to constrain temperature-  
82 index model parameters (e.g. Rounce and others, 2020a, 2023; Compagno and others, 2021). However, these  
83 observations represent multi-year signals of mass change, integrated over the glacier area, and are afflicted  
84 with relatively large uncertainties. Therefore, these multi-year geodetic data provide only coarsely-resolved  
85 spatiotemporal variability and limited constraints on model parameters (Sjursen and others, 2023), such

86 that mass-balance models still require seasonal mass-balance signals to adequately constrain accumulation  
87 and ablation.

88 The goal of this work is to provide a reconstruction of the surface mass balance (SMB) of Jostedalbreen  
89 ice cap from 1960–2020 that is coherent in space and time, and in line with several observational datasets.  
90 We aim to capture the spatiotemporal variability in SMB in detail over seasonal time scales and to assess  
91 SMB variability in response to potential climatic and topographic drivers. To achieve this, we model  
92 the SMB of Jostedalbreen using a temperature-index model forced by high-resolution (1 km) daily mean  
93 temperature and daily total precipitation from the seNorge\_2018 dataset (Lussana and others, 2019). To  
94 ensure that the modelled SMB conforms with observational datasets we employ a Bayesian framework to  
95 estimate model parameters in a two-step procedure: 1) seasonal glaciological mass-balance measurements  
96 are used to estimate a global model parameter set that constrains accumulation and ablation on the ice  
97 cap, and 2) the global parameter set is employed as prior to estimate glacier-specific parameter sets using  
98 geodetic mass-balance observations for each glacier. The procedure allows us to quantify the uncertainty in  
99 simulated SMB that arises from uncertainty in model parameters and other sources such as uncertainties  
100 that arise from limitations in the model structure and input data. We thus demonstrate an approach  
101 that leverages observational datasets with complementary mass-balance information to provide robust  
102 spatiotemporal SMB estimates across a diverse region.

## 103 2 STUDY AREA AND DATA

### 104 2.1 Study area

105 Jostedalbreen stretches along a south-west to north-east axis in western Norway (Fig. 1), covering an area  
106 of 458 km<sup>2</sup> in 2019 (Andreassen and others, 2022) and with an estimated volume of 70.6 km<sup>3</sup> (~2020;  
107 Gillespie and others, 2024). In the latest glacier inventory (2019) the ice cap is divided into 81 glaciers  
108 ranging in area from less than 0.1 km<sup>2</sup> to 46.2 km<sup>2</sup> (Tunsbergdalsbreen; Andreassen and others, 2022).  
109 In previous inventories (1966; Winsvold and others (2014), 2006; Andreassen and others (2012)) the ice  
110 cap was divided into 82 units, but two disconnected units were removed and one was added in the 2019  
111 inventory (Andreassen and others, 2023). In this work we consider the 82 glaciers from the 1966 and 2006  
112 inventories.

113 Jostedalbreen consists of three main parts that are connected by relatively narrow bands of ice (Gille-  
114 spie and others, 2024). The three parts are hereafter referred to as North (north-east of Lodalsbreen,

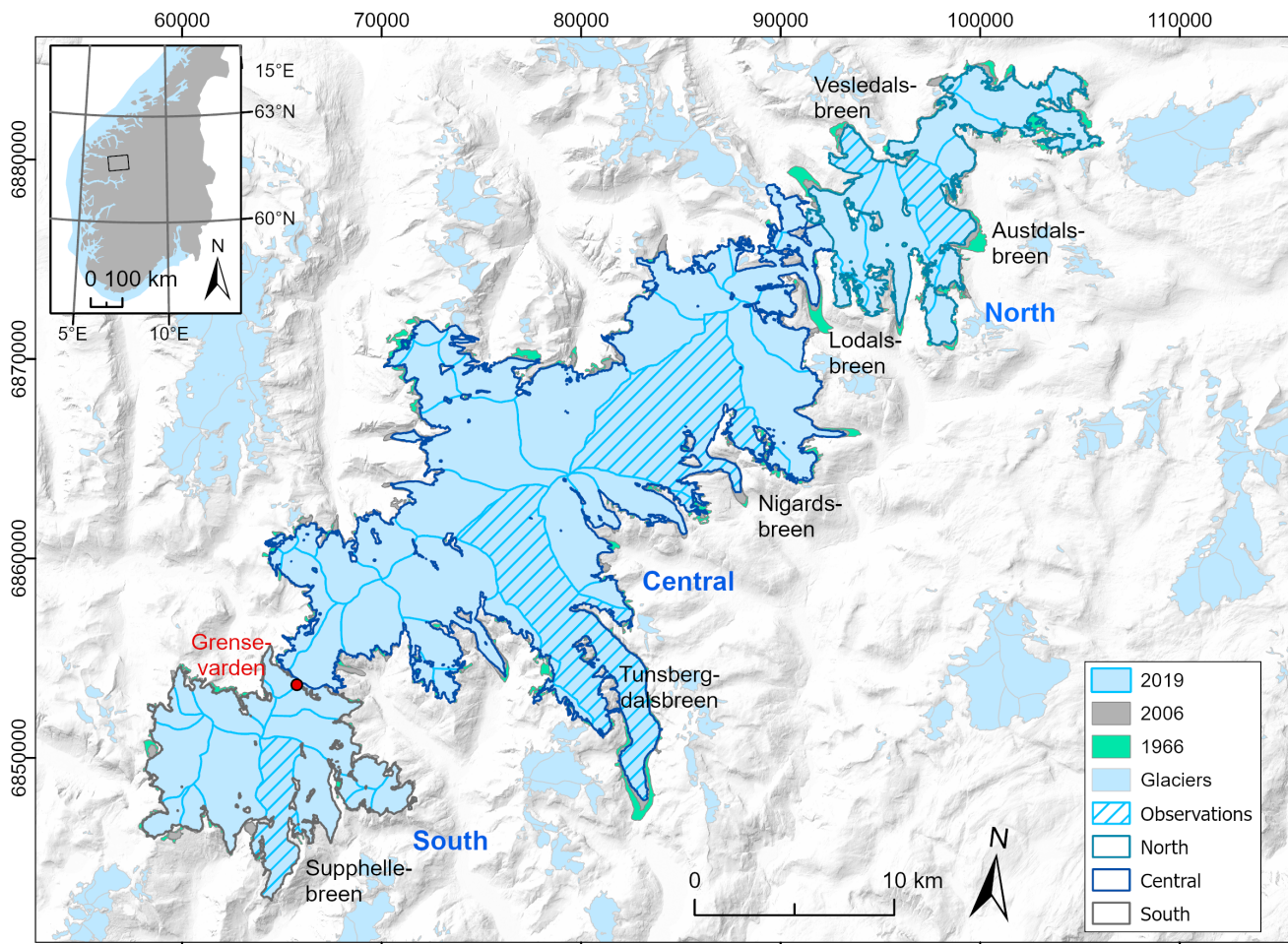


**Fig. 1.** Overview of Jostedal ice cap in western Norway with glacier outlines from 1966 (Winsvold and others, 2014), 2006 (Andreassen and others, 2012), and 2019 (Andreassen and others, 2022). Hatched areas show glaciers with glaciological surface mass-balance observations. The coordinate systems are geographical coordinates on the inset and UTM33N, datum ETRS89 on main map.

115 Norwegian Water Resources and Energy Directorate (NVE) glacier ID2266; 24 glaciers), South (south of  
 116 Grensevarde/ID2332; 19 glaciers), and Central (39 glaciers; Fig. 1) following Gillespie and others (2024),  
 117 see list of IDs in Appendix A. Surface elevation extends from below 400 m a.s.l. at the tongues of the  
 118 largest outlet glaciers to above 1900 m a.s.l. on the ice cap plateau. The north-western side of the ice cap  
 119 is characterized by mainly short and steep glaciers, while the south-eastern side holds several large valley  
 120 glaciers, of which Nigardsbreen is most extensively studied (e.g. Østrem and others, 1976; Oerlemans, 1997;  
 121 Engelhardt and others, 2014; Li and others, 2015; Gjerde and others, 2023).



## 122 2.2 Mass-balance data and glacier inventory

123 Observations of mass change on Jostedalsbreen during the past 60 years are available from several sources  
124 with different spatial coverage and temporal resolution. Glaciological SMB measurements have been per-  
125 formed by NVE on parts of the ice cap since the early 1960s (Table 1; e.g. Kjølmoen and others, 2022).  
126 The outlet glaciers Nigardsbreen and Austdalsbreen have continuous long-term SMB records since the  
127 mass-balance years 1962 and 1988, respectively, providing observations of annual and seasonal (winter and  
128 summer) SMB over 59 (1962–2020) and 33 (1988–2020) consecutive mass-balance years over the study  
129 period (Kjølmoen and others, 2022). Note that when referring to mass-balance years, we refer to the year  
130 marking the end of a mass-balance year (e.g. 1962 refers to the mass-balance year 1961/62). Three other  
131 glaciers have shorter SMB records: Tunsbergdalsbreen (1966–1972; 7 years), Vesledalsbreen (1967–1972;  
132 6 years), and Supphellebreen (1964–1967, 1973–1975, 1979–1982; 11 years; Kjølmoen, 2017). Mass loss  
133 due to lake-calving is generally negligible for Jostedalsbreen, except for Austdalsbreen where calving is  
134 estimated annually by NVE and reported to account for up to 20% of the annual ablation (e.g. Kjølmoen  
135 and others, 2022).

136 Of the five original glaciological SMB records, four have been homogenized: Nigardsbreen, Austdals-  
137 breen, Tunsbergdalsbreen, and Vesledalsbreen (Andreassen and others, 2016; Kjølmoen, 2017, 2022) and  
138 Nigardsbreen has been partly calibrated due to significant differences between geodetic and glaciologi-  
139 cal mass-balance records (Andreassen and others, 2016; Kjølmoen, 2022). Supphellebreen has not been  
140 homogenised due to lack of data (Kjølmoen, 2017). In this study, we consider the homogenized and  
141 calibrated records for all glaciers except for Supphellebreen, where we use the original record. For Nigards-  
142 breen, glaciological SMB is measured for the basin consisting of Nigardsbreen (ID2297) and two smaller  
143 glaciers (ID2299 and 2311). In this study, we employ the same basin as the glaciological record when  
144 comparing modelled and glaciological SMB for Nigardsbreen.

145 Geodetic mass balance estimates are available for Jostedalsbreen, or parts of the ice cap, for time  
146 periods of various length. Satellite-borne geodetic mass balance from repeat ASTER Digital Elevation  
147 Models (DEMs) is available for all glaciers for the period 2000–2019 (Hugonnet and others, 2021). In  
148 addition, geodetic mass balance is available for 49 glaciers for the period 1966–2020 (Andreassen and others,  
149 2023). The latter estimates are based on aerial photographs from 1966 and airborne LiDAR surveys in  
150 2020, and cover central and northern parts of the ice cap. Geodetic mass balance for Nigardsbreen,  
151 Tunsbergdalsbreen, and Austdalsbreen is also available for other periods (e.g. Andreassen and others,

**Table 1.** Overview of glaciological surface mass-balance (SMB) observations for glaciers of Jostedalbreen used in this study. ID refers to the Norwegian Water Resources and Energy Directorate (NVE) glacier ID (Andreassen and others, 2022). Location refers to glacier location in the South (S), Central (C), or North (N) part of the ice cap. Area and elevation range (min–max) refer to the 2019 inventory (Andreassen and others, 2022).  $n_{ann}$  and  $n_{seas}$  are the respective number of mass-balance years with annual and seasonal glaciological SMB observations for each glacier over the study period 1960–2020 (e.g. Kjølmoen, 2017; Kjølmoen and others, 2022; Andreassen and others, 2020). Period refers to the time period covered by SMB observations (mass-balance years). Glaciological SMB measurements for Nigardsbreen includes ID2297, 2299 and 2311.

ID	Name	Location	Area km <sup>2</sup>	Elevation range m a.s.l.	Aspect	$n_{ann}$	$n_{seas}$	Period
2297	Nigardsbreen	C	41.71	345–1946	SE	59	59	1962–2020
2478	Austdalsbreen	N	10.27	1222–1755	SE	33	33	1988–2020
2320	Tunsbergdalsbreen	C	46.23	656–1930	SE	7	7	1966–72
2352	Supphellebreen	S	12.72	733–1734	S	11	4	1964–67, 73–75, 79–82
2474	Vesledalsbreen	N	3.19	1221–1757	NW	6	6	1967–72

152 2016, 2020, 2023), but are not included in this study since they provide limited additional information.

153 Glacier outlines required for modelling SMB of Jostedalbreen and individual glaciers are available from  
 154 1966 (Winsvold and others, 2014), 2006 (Andreassen and others, 2012) and 2019 inventories (Andreassen  
 155 and others, 2022). Ice divides in the 2019 inventory are mostly aligned with 2006 outlines but updated  
 156 for some glaciers (Nigardsbreen, Austdalsbreen and neighboring glaciers) to harmonize with those used in  
 157 glaciological SMB calculations (Andreassen and others, 2022; Kjølmoen, 2022). The 1966 ice divides have  
 158 been homogenised with the 2019 inventory (Andreassen and others, 2023). Additional glacier outlines used  
 159 in calculation of glaciological SMB are available for Nigardsbreen (1964, 1974, 1984, 2009, 2013, 2020) and  
 160 Austdalsbreen (1988, 2009) (e.g. Kjølmoen and others, 2022).

### 161 2.3 Meteorological forcing data

162 As meteorological forcing for the SMB model we employ gridded 1 km resolution daily mean temperature  
 163 and daily total precipitation from seNorge\_2018 version 21.09 (Lussana and others, 2019; Lussana, 2021).  
 164 The seNorge (<https://www.senorge.no/>) collection of datasets are provided by the Norwegian Meteorolog-  
 165 ical Institute (MET Norway) and are based on spatial interpolation of measurements from a large network  
 166 of weather stations across the Norwegian mainland, while also leveraging monthly precipitation reference  
 167 fields from 3 km climate model simulations from HARMONIE to improve precipitation estimates in data-  
 168 sparse regions (Lussana and others, 2019; Lussana, 2020). Several versions of seNorge (e.g. seNorge1.1

169 (Mohr, 2008) and seNorge\_2018 (Lussana and others, 2019)) have previously been applied in SMB and  
 170 runoff modelling of glacierized areas in Norway (e.g. Engelhardt and others, 2013, 2014; Li and others,  
 171 2015; Sjursen and others, 2023), and to correct downscaled climate model projections in assessments of  
 172 climate-change impacts (Wong and others, 2016; Hanssen-Bauer and others, 2017). Overall, seNorge\_2018  
 173 is considered to improve precipitation estimates compared to its predecessors. Nevertheless, the probabil-  
 174 ity of large errors is considered greatest for precipitation in remote, mountainous regions with low station  
 175 density (Lussana and others, 2019), where glaciers commonly reside.

## 176 3 METHODS

### 177 3.1 Surface mass-balance model

The surface mass balance of a glacier over a given period (e.g. year, season) is the sum of accumulation and ablation on its surface (Cogley and others, 2011). Accumulation at Jostedalbreen is mainly in the form of snowfall, while surface ablation is mainly melt of snow, firn and ice. We calculate the SMB of Jostedalbreen on the 1 km resolution DEM of the seNorge dataset. We use the temperature-index model (see e.g. Hock, 2005) employed in Sjursen and others (2023), where melt of snow or ice in a grid cell  $i$  at the daily time step  $t$ ,  $m_{snow/ice,i,t}$  (mm w.e. °C<sup>-1</sup>d<sup>-1</sup>), is computed using melt factors for snow and ice,  $MF_{snow/ice}$ , when the mean daily temperature in a grid cell  $T_{i,t}$  is above a melt threshold temperature ( $T_m = 0$  °C):

$$m_{snow/ice,i,t} = \begin{cases} MF_{snow/ice}(T_{i,t} - T_m) & \text{if } T_{i,t} > T_m, \\ 0 & \text{if } T_{i,t} \leq T_m. \end{cases} \quad (1)$$

178 Firn melt is estimated as the average of daily melt of snow and ice, since the albedo of firn is typically  
 179 between that of snow and ice (Cuffey and Paterson, 2010). To account for differences in albedo between  
 180 snow and ice, we set  $MF_{ice} = MF_{snow}/0.7$ . Thereby we assume that the melt rate for clean snow is  
 181 70% of that of clean ice (e.g. Singh and others (2000), in line with calibrated values for all glaciers in  
 182 Norway Engelhardt and others (2013)). Daily accumulation in a grid cell is computed as the fraction of  
 183 the daily total precipitation in the cell falling as snow, assuming a linear decrease from entirely solid to  
 184 liquid in a  $\pm 1$  °C interval around 1 °C (Jennings and others, 2018). We evaluate mass changes of the ice  
 185 cap over a hydrological year (1 October–30 September, with 30 April as end of accumulation season). In  
 186 model calibration and validation we assess mass changes based on dates of maximum and minimum mass



187 for a more accurate comparison to available observations of individual glaciers (e.g. glaciological SMB is  
188 measured for end of accumulation/melt seasons).

189 Due to the uncertainty in the meteorological forcing data, we add a temperature correction  $T_{corr}$  ( $^{\circ}\text{C}$ )  
190 to the daily mean temperature and multiplying the daily total precipitation by a precipitation correction  
191 factor  $P_{corr}$  (-). The unknown model parameters are thus  $MF_{snow}$ ,  $P_{corr}$  and  $T_{corr}$ , whose values are  
192 constrained using the Bayesian framework described in Section 3.2.

### 193 3.2 Bayesian parameter estimation

194 We employ a Bayesian framework (see e.g. Gelman and others, 2014) to estimate probability distributions  
195 of the SMB model parameters and to quantify uncertainty in modelled SMB. Our procedure consists of  
196 two steps that leverage two different observational datasets and aims to estimate model parameters that  
197 constrain accumulation and ablation on Jostedalbreen (step 1), while also providing accurate estimates of  
198 SMB for each individual glacier (step 2). These steps are first summarized below, before we describe the  
199 details of each step in Sections 3.2.1 and 3.2.2.

200 In step 1 we estimate a global parameter set  $\theta = \{P_{corr, glob}, T_{corr, glob}, MF_{snow, glob}\}$  that most accurately  
201 represents the SMB of the entire ice cap, constrained by seasonal glaciological SMB observations from  
202 five glaciers (Table 1). We also estimate the distribution of a model error that is not accounted for by  
203 the model parameters and represents the structural model uncertainty (e.g. due to missing or simplified  
204 process representation) and uncertainty in the input data. This allows us to properly quantify the predictive  
205 uncertainty of the model and provide robust SMB estimates.

206 In step 2 we spatially adjust the precipitation and temperature correction parameters recovered in  
207 step 1, by estimating a set of glacier-specific precipitation and temperature correction parameters  $\phi_j =$   
208  $\{P_{corr, j}, T_{corr, j}\}$  for each glacier  $j$ . To this end, we employ two decadal geodetic mass-balance observations  
209 for each glacier (2000–09 and 2010–19) from Hugonnet and others (2021) since this dataset covers the entire  
210 ice cap. To estimate  $\phi_j$ , we use the posterior distributions of  $P_{corr, glob}$  and  $T_{corr, glob}$  obtained from step  
211 1 as the prior distributions in step 2. The geodetic observations have low temporal resolution and high  
212 uncertainty, and posterior estimates can therefore be expected to be strongly influenced by the choice of  
213 prior distribution (Sjursen and others, 2023). We mitigate this by using posterior distributions from step  
214 1 as priors in step 2, which represent reliable estimates of accumulation and ablation.

215 In step 2 we fix  $MF_{snow}$  to the median of the posterior distribution of  $MF_{snow, glob}$  and thus choose to

216 spatially adjust two parameters that each mainly controls either accumulation (precipitation correction) or  
 217 ablation (temperature correction) (Réveillet and others, 2017). This is because the geodetic observations  
 218 provide limited information to constrain strongly correlated parameters (e.g. temperature correction and  
 219 melt factor; Rounce and others, 2020b; Sjursen and others, 2023). Furthermore, we expect that spatial  
 220 patterns of temperature and precipitation may not be accurately represented in seNorge\_2018 due to the  
 221 complex topography of the region and significant local effects on weather patterns. In step 2 we thus address  
 222 possible spatial biases in the meteorological forcing data over the ice cap, by adjusting the well-constrained  
 223 parameter values in step 1.

### 224 3.2.1 Step 1: Estimation of global parameter set and model error

We formulate a deterministic model (Eqn. 2) that is similar to those of Rounce and others (2020b) and Sjursen and others (2023), but that also takes into account that the SMB model is an imperfect representation of an observed system. That is, instead of assuming that the model describes the observed system up to an observation error  $\epsilon_n$ , we include an additional unknown model error  $\eta_n$ :

$$B_{obs,n} = B_{mod,n}(X_n, \theta) + \epsilon_n + \eta_n, \quad (2)$$

where  $B_{obs,n}$  and  $B_{mod,n}(X_n, \theta)$  are observed and modelled SMB over  $n$  periods of mass change, respectively, and  $X_n$  is the set of model input data. Here,  $\eta_n$  is meant to represent any predictive uncertainty that is not accounted for by parameter uncertainty. This includes uncertainty in the model structure, e.g. from missing or crudely parameterized physical processes, but also other sources of uncertainty that are not accounted for otherwise. We consider  $\epsilon_n$  and  $\eta_n$  to be statistically independent since there is no physical relation between these errors. Further, we assume  $\epsilon_n$  and  $\eta_n$  to be normally distributed ( $\mathcal{N}$ ) with means of zero and constant variances. The variance of the distribution of  $\epsilon_n$  is given by the uncertainty in the SMB observation  $\sigma_{B_{obs}}^2$ , while  $\eta_n$  has unknown variance  $\sigma_\eta^2$ :

$$\epsilon_n \sim \mathcal{N}(0, \sigma_{B_{obs}}^2), \quad (3)$$

$$\eta_n \sim \mathcal{N}(0, \sigma_\eta^2). \quad (4)$$

We employ Markov chain Monte Carlo (MCMC) simulations that make use of the following proportionality in Bayes' theorem to estimate the joint posterior distribution of  $\theta$  and  $\sigma_\eta$  given a set of mass-balance observations  $B_{obs,1:N}$  and input data  $X_{1:N}$ :

$$p(\theta, \sigma_\eta | B_{obs,1:N}, X_{1:N}) \propto p(\theta) p(\sigma_\eta) L_{B_{obs}}, \quad (5)$$

225 where  $p$  denotes probability and  $L_{B_{obs}} = p(B_{obs,1:N} | \theta, \sigma_\eta, X_{1:N})$  is termed the likelihood: the probability of  
 226 observing the data  $B_{obs,1:N}$  given our deterministic model (Eqn. 2). In MCMC simulations we employ the  
 227 logarithm of the likelihood function  $l_{B_{obs}} = \ln(L_{B_{obs}})$  to ensure stability and efficient computation. Under  
 228 the assumption of independent and normally distributed errors with constant variances, we formulate the  
 229 log-likelihood as follows:

$$l_{B_{obs}} = -\frac{N}{2} \ln(2\pi) - \frac{N}{2} \ln(\sigma_{B_{obs}}^2 + \sigma_\eta^2) - \frac{1}{2(\sigma_{B_{obs}}^2 + \sigma_\eta^2)} \sum_{n=1}^N (B_{obs,n} - B_{mod,n}(X_n, \theta))^2. \quad (6)$$

We employ seasonal SMB observations such that the modelled SMB  $B_{mod,n}$  over the period  $n$  is the modelled summer or winter SMB, and  $B_{obs,n}$  the SMB observation for the same period, with associated uncertainty  $\sigma_{B_{obs}}$ . We assume that seasonal SMB observations are conditionally independent given our model, such that we can express the full log-likelihood function  $l_{B_{seas}}$  as the sum of the log-likelihood functions for each of winter and summer SMB ( $l_{B_w}$  and  $l_{B_s}$ , respectively):

$$l_{B_{seas}} = l_{B_w} + l_{B_s}, \quad (7)$$

230 where  $l_{B_w}$  and  $l_{B_s}$  are given by Equation 6.

231 For estimation of the global model parameter set  $\theta = \{P_{corr, glob}, T_{corr, glob}, MF_{snow, glob}\}$  and the standard  
 232 deviation in model error  $\sigma_\eta$ , we employ seasonal glacier-wide glaciological SMB observations (Table 1) for  
 233 every other mass-balance year of the period 1962–2020 (even years, starting with mass-balance year 1962  
 234 and ending with 2020), totalling 56 mass-balance years of winter and summer SMB for the five glaciers.  
 235 We use annual and seasonal SMB observations for the remaining 53 mass-balance years for validation  
 236 of posterior predictive SMB. When comparing modelled SMB to observations from Nigardsbreen and  
 237 Austdalsbreen, we employ the same time-series of glacier outlines as used in glaciological records (for

shorter records the 1966 outline is considered representative).

Following Sjursen and others (2023), we determine the uncertainty in seasonal glacier-wide glaciological SMB based on estimates from the reanalysis of the long-term glaciological SMB records in Norway (Andreassen and others, 2016), assuming that observations of summer and winter SMB are independent (Dyurgerov and Meier, 1999) and that the uncertainty in summer SMB accounts for two-thirds of the uncertainty of glacier-wide annual SMB (e.g. Kjöllmoen and others, 2022). Uncertainty in glacier-wide annual SMB is estimated to  $\pm 0.34$  m w.e.a<sup>-1</sup> and  $\pm 0.30$  m w.e.a<sup>-1</sup> for Nigardsbreen (1964–2013) and Austdalsbreen (1988–2009), respectively (Andreassen and others, 2016). Individual error estimates are lacking for the short-term glaciological SMB records on Jostedalsbreen, but are considered to be of similar magnitude as the long-term series (Kjöllmoen, 2017). For simplicity, we assume that the estimated uncertainty in glacier-wide annual SMB measurements for Nigardsbreen is representative for all glaciers;  $\sigma_{B_w} = 0.19$  m w.e.a<sup>-1</sup> and  $\sigma_{B_s} = 0.28$  m w.e.a<sup>-1</sup> for winter and summer SMB, respectively (Sjursen and others, 2023).

### 3.2.2 Step 2: Estimation of glacier-specific precipitation and temperature correction

Our deterministic model for step 2 is similar to step 1 (Eqn. 2), but applied to each glacier individually with  $\epsilon_{n,j} \sim \mathcal{N}(0, \sigma_{B_{obs,n,j}}^2)$ . For the model error we assign a decadal model uncertainty  $\sigma_{\eta,10yr}$  from the posterior mean of  $\sigma_{\eta}$ , given that  $\sigma_{\eta}$  is the model uncertainty associated with a seasonal SMB prediction. The log-likelihood function for each glacier  $j$  in step 2 is thus:

$$l_{B_{obs,10yr,j}} = l_{B_{obs,00-09,j}} + l_{B_{obs,10-19,j}}, \quad (8)$$

where  $l_{B_{obs,10yr,j}}$  is the combined log-likelihood for the geodetic mass-balance observations of glacier  $j$  over each of the periods 2000–09 ( $N=00-09$ ) and 2010–19 ( $N=10-19$ ), and is given by:

$$l_{B_{obs,N,j}} = -\frac{1}{2} \ln(2\pi) - \frac{1}{2} \ln(\sigma_{B_{obs,N,j}}^2 + \sigma_{\eta,10yr}^2) - \frac{1}{2(\sigma_{B_{obs,N,j}}^2 + \sigma_{\eta,10yr}^2)} (B_{obs,N,j} - B_{mod,N,j}(X_j, \phi_j))^2. \quad (9)$$

For each decadal geodetic mass-balance observation we assign the uncertainty  $\sigma_{B_{obs,N,j}}$  reported by Hugonnet and others (2021) for a given period  $N$  and glacier  $j$ . Similar to step 1, we employ MCMC simulations to estimate the posterior of  $\phi_j = \{P_{corr,j}, T_{corr,j}\}$  for each glacier (see Appendix B for details).

## 257 3.2.3 Posterior predictive SMB simulations

We perform posterior predictive SMB simulations using posterior distributions of step 1, but with posterior means of global parameters  $P_{corr, glob}$  and  $T_{corr, glob}$  corrected to posterior means of  $P_{corr, j}$  and  $T_{corr, j}$  estimated in step 2. This allows us to run posterior predictive simulations for the deterministic model described in Equation 2 with posterior estimates of  $MF_{snow, glob}$  and  $\eta_n$ , but with spatial adjustment of posteriors of  $P_{corr, glob}$  and  $T_{corr, glob}$ . More specifically, for each glacier we adjust the posterior of the global precipitation correction  $P_{corr, glob}$  by  $c_j = \mu_{P_{corr, j}} - \mu_{P_{corr, glob}}$  the difference between the means of  $P_{corr, j}$  and  $P_{corr, glob}$ , respectively:

$$P_{corr, glob} + c_j \sim \mathcal{N}(\mu_{P_{corr, glob}} + c_j, \sigma_{P_{corr, glob}}^2). \quad (10)$$

258 We perform a corresponding operation for temperature correction using  $T_{corr, glob}$  and  $T_{corr, j}$ . The underlying  
259 assumption in Equation 10 is that posterior distributions of  $P_{corr, glob}$  and  $T_{corr, glob}$  are approximately  
260 normal, which is demonstrated in Section 4.1.

261 In posterior predictive simulations we employ the set of outlines from 1966, 2006 and 2019, and follow  
262 the principle applied in homogenization of glaciological SMB records in Norway of using each outline for  
263 half of the period before and after its date (Andreassen and others, 2016).

## 264 3.2.4 Prior distributions for global parameter set

265 As prior distribution for  $P_{corr, glob}$  we choose a normal distribution truncated at zero (to ensure positivity),  
266 with mean of 1.0 and standard deviation of 0.25 as the prior distribution. Although previous evaluation  
267 reveals that precipitation estimates over outlet glaciers of Jostedalbreen (Nigardsbreen and Austdalsbreen)  
268 may be underestimated in seNorge\_2018 (Sjursen and others, 2023), we do not know if estimates of  
269 precipitation correction factors (based on observations from 1990–2009 for Austdalsbreen and Nigardsbreen)  
270 are representative for the whole ice cap over the period 1960–2020. Our choice of prior for  $P_{corr, glob}$  gives  
271 95% confidence interval limits at approximately 0.5 and 1.5, meaning that we are confident that the  
272 under- or overestimation of precipitation sums over Jostedalbreen do not exceed 50%. Since there are no  
273 indications of bias or large errors in daily mean temperature in seNorge\_2018 (Lussana and others, 2019),  
274 we choose a normal distribution with mean±standard deviation of  $0 \pm 0.5$  °C (95% confidence interval  
275 limits at approximately  $\pm 1$  °C) for the prior distribution of  $T_{corr, glob}$ .

276 Similarly to Rounce and others (2020b) and Sjursen and others (2023) our choice of prior for  $MF_{snow, glob}$   
277 is based on Braithwaite (2008), who found a value of  $4.1 \pm 1.5$  mm w.e.  $^{\circ}\text{C}^{-1}\text{d}^{-1}$  for the melt factor for snow  
278 at the equilibrium line altitude (ELA) of 66 glaciers. However, in light of previous parameter estimates for  
279 outlet glaciers of Jostedalsbreen (Sjursen and others, 2023), we believe that values are more likely closer  
280 to the mean and therefore adopt a zero-truncated normal distribution with mean  $\pm$  standard deviation of  
281  $4.1 \pm 1.0$  mm w.e.  $^{\circ}\text{C}^{-1}\text{d}^{-1}$  (95% confidence interval at 2.1 and 6.1 mm w.e.  $^{\circ}\text{C}^{-1}\text{d}^{-1}$ ) as prior distribution  
282 for  $MF_{snow, glob}$ .

283 As the prior for the standard deviation of the model error  $\sigma_{\eta}$  we choose a half-normal distribution  
284 since the standard deviation is a positive number and because we believe that there is a high probability  
285 of small errors and a low probability of very large errors. Further, we choose a scale parameter of 0.67 for  
286 the half-normal distribution such that the model error is likely (95% confidence interval) within 1.5 m w.e.,  
287 which reflects the reported error distribution in studies with similar SMB model set-up (Huss and Hock,  
288 2015).

## 289 4 RESULTS

290 In this section we show the posterior parameter distributions resulting from our two-step parameter estima-  
291 tion procedure (Section 4.1) and present the simulated SMB of Jostedalsbreen from 1960–2020, highlighting  
292 both the spatial and temporal variability (Section 4.2). Unless specified otherwise, reported SMB is based  
293 on simulations with 1000 posterior predictive samples of the posterior distribution shown in Section 4.1.

### 294 4.1 Posterior parameter estimates

295 We find that posterior distributions of  $\theta = \{P_{corr, glob}, T_{corr, glob}, MF_{snow, glob}\}$  and  $\sigma_{\eta}$  in step 1 of parameter  
296 estimation are well constrained (Fig. 2). The posterior of the precipitation bias correction ( $P_{corr, glob}$ ) has a  
297 mean/median  $\pm$  standard deviation of  $1.25/1.25 \pm 0.04$ , and naturally shows the lowest spread since it has  
298 limited correlation to other parameters and is informed by winter SMB observations. The corresponding  
299 statistics for the posterior of the melt factor for snow ( $MF_{snow, glob}$ ) is  $3.58/3.56 \pm 0.25$  mm w.e.  $^{\circ}\text{C}^{-1}\text{d}^{-1}$   
300 and  $-0.14/-0.14 \pm 0.34$   $^{\circ}\text{C}$  for the temperature bias correction ( $T_{corr, glob}$ ), both shifted towards slightly  
301 lower-ablation values compared to prior distributions.

302 The mean/median  $\pm$  standard deviation of the posterior distribution of model uncertainty (i.e. standard  
303 deviation in model error,  $\sigma_{\eta}$ ) is  $0.32/0.32 \pm 0.04$  m w.e. The model uncertainty reflects the error in modelled



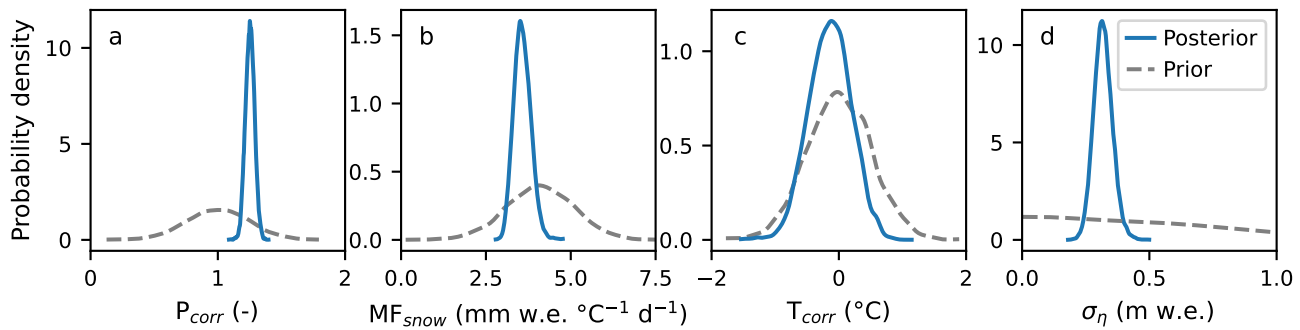


**Fig. 2.** Marginal prior (grey dashed lines) and posterior (blue solid lines) probability distributions of global parameter set: (a) precipitation correction factor  $P_{corr, glob}$ , (b) melt factor for snow  $MF_{snow, glob}$ , and (c) temperature bias correction  $T_{corr, glob}$ , and (d) standard deviation in model error  $\sigma_\eta$ .

304 glacier-wide seasonal SMB (Eqn. 2), and is slightly higher than the uncertainty in observed glacier-wide  
 305 winter and summer SMB from glaciological records. The error in modelled glacier-wide annual SMB can  
 306 be estimated as the sum of normally distributed errors (following our assumption in Equation. 4), such  
 307 that  $\eta_{B_{mod,a}} \sim \mathcal{N}(0, 0.45^2)$  m w.e.

308 Overall, posterior distributions of spatially corrected  $P_{corr,j}$  from step 2 display lower values (lower  
 309 precipitation sums) compared to  $P_{corr, glob}$ , while posteriors of  $T_{corr,j}$  are mostly shifted towards higher  
 310 values (higher temperature) compared to  $T_{corr, glob}$  (Fig. 3). The minimum/maximum value of the medians  
 311 of the posteriors of  $P_{corr,j}$  and  $T_{corr,j}$  are 1.20/1.27 and -1.06/0.98 °C, respectively. Posteriors show spatial  
 312 patterns across Jostedalbreen, with higher values of  $P_{corr,j}$  (higher precipitation sums) on the south-eastern  
 313 side and in northern parts of the ice cap (Fig. 3a) and higher values of  $T_{corr,j}$  on the north-western side  
 314 and in the south (Fig. 3b). However, there are some local variations to these patterns, e.g. the smaller  
 315 glaciers in the central north-western region that shows high values of  $P_{corr,j}$  and low values of  $T_{corr,j}$ .

## 316 4.2 Mass balance of Jostedalbreen 1960–2020

317 Overall, the modelled SMB of Jostedalbreen is slightly negative over the period 1960–2020 (Fig. 4). We  
 318 find a median cumulative SMB of -4.05 m w.e (95% credible interval (CI): -12.52, 5.12 m w.e), equivalent to  
 319 an annual SMB rate of -0.07 m w.e. a<sup>-1</sup> (95% CI: -0.21, 0.08 m w.e. a<sup>-1</sup>). The median summer and winter  
 320 SMB rates over the model period are -2.10 m w.e. a<sup>-1</sup> (95% CI: -2.19, 2.00 m w.e. a<sup>-1</sup>) and 2.02 m w.e. a<sup>-1</sup>  
 321 (95% CI: 1.92, 2.14 m w.e. a<sup>-1</sup>), respectively. Considering individual glaciers over the period 1960–2020,  
 322 annual SMB rates are generally slightly positive for glaciers in the south-western part of Jostedalbreen,  
 323 close to zero for glaciers in the central part and overall negative for glaciers in the north-east (Fig. 5a). Some

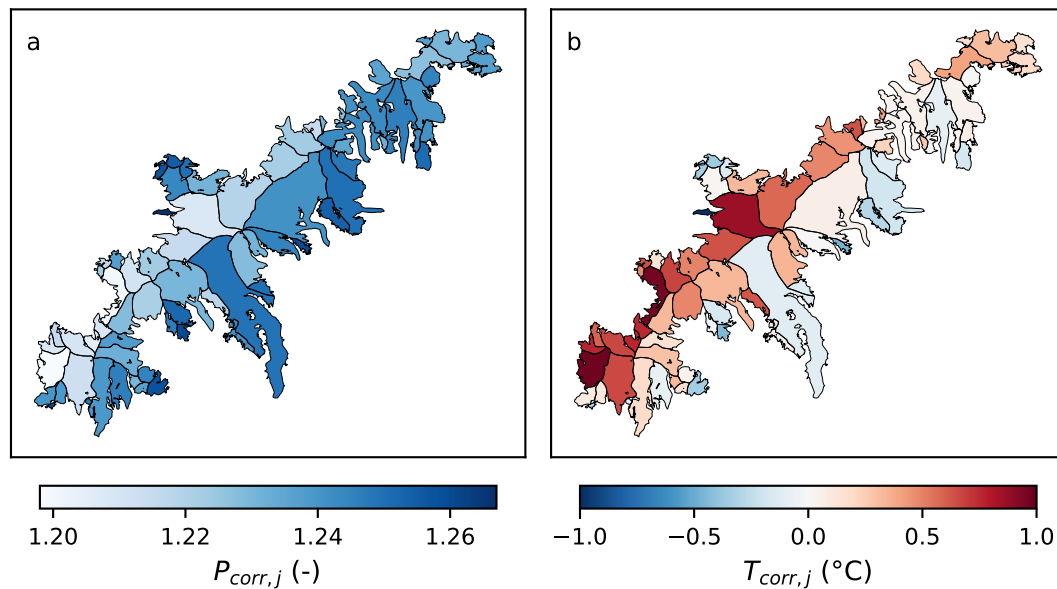


**Fig. 3.** Median values of marginal posterior probability distributions of (a)  $P_{corr,j}$  and (b)  $T_{corr,j}$  for each glacier  $j$  of Jostedalbreen.

324 smaller glaciers at the margins of the central and south-western parts of the ice cap also display negative  
 325 SMB. The largest outlet glaciers Tunsbergdalsbreen and Nigardsbreen show negative annual SMB rates of  
 326  $-0.43 \text{ m w.e. a}^{-1}$  (95% CI:  $-0.62, -0.23 \text{ m w.e. a}^{-1}$ ) and  $-0.09 \text{ m w.e. a}^{-1}$  (95% CI:  $-0.26, -0.12 \text{ m w.e. a}^{-1}$ ),  
 327 respectively.

328 Our model results reveal that Jostedalbreen has experienced both periods of mass loss and gain over  
 329 the past 60 years, with large temporal variability (Fig. 4 and Table 2). In the 1960s, the ice cap experienced  
 330 significant mass loss, followed by a relatively stable period from the 1970s until the mid-1980s. From the  
 331 end of the 1980s and throughout the 1990s the ice cap gained mass, followed by a mass deficit of similar  
 332 magnitude from 2000 until the mid-2010s. From the mid-2010s, the mass of Jostedalbreen has again been  
 333 relatively stable according to our model results. Considering magnitudes of decadal variations in SMB of  
 334 the ice cap (Table 2), the 1980s and 1990s are the only positive decades, with the 1990s showing the largest  
 335 mass gain. The positive SMB over these two decades is driven by relatively low magnitude of summer SMB  
 336 (85 and 92% of the average for 1960–2020, respectively) and higher-than-average magnitude of winter SMB  
 337 in the 1990s (130%). The most negative decade in terms of annual SMB rate over the ice cap is the 1960s,  
 338 followed by the most recent decades 2000–09 and 2010–19. The 1960s display average summer SMB, but  
 339 very low winter SMB over the ice cap (73%). In contrast, the 2000s and 2010s show average winter SMB  
 340 rates, with overall negative annual rates dominated by high magnitudes of summer SMB (118 and 109%,

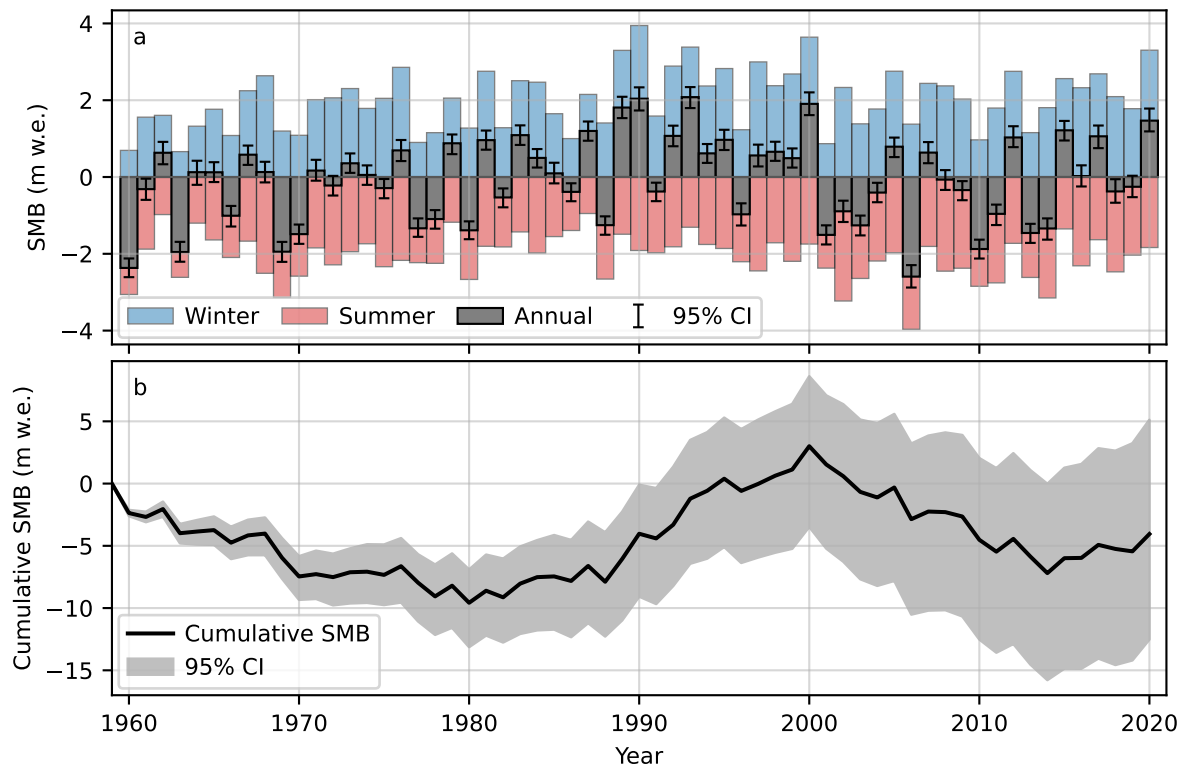


**Fig. 4.** (a) Median glacier-wide annual (grey, whiskers represent 95% credible interval (CI)), winter (blue) and summer (red) surface mass balance (SMB; m w.e.) of Jostedalsgreen over the period 1960–2020, based on 1000 posterior predictive samples. (b) Cumulative SMB for the ice cap from 1960–2020, based on median of 1000 posterior predictive samples (shaded area represents 95% CI).

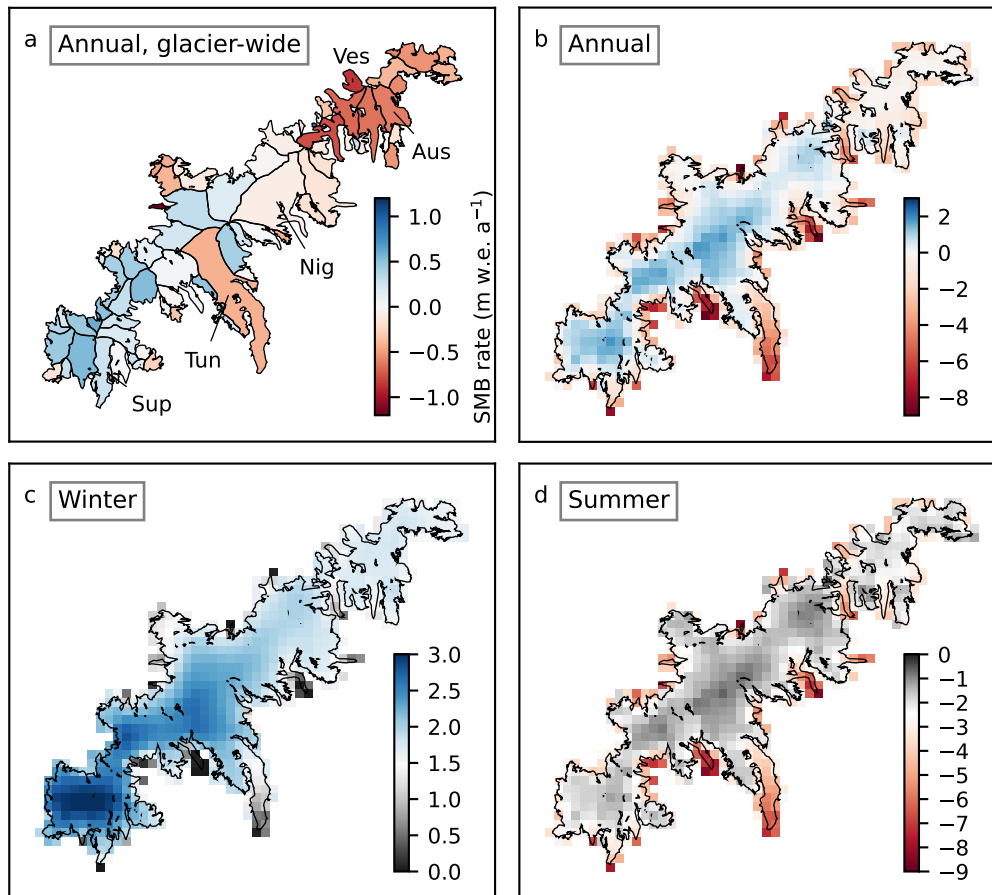


**Fig. 5.** (a) Glacier-wide annual average surface mass balances (median SMB in m w.e. a<sup>-1</sup>) using 1000 posterior predictive samples and gridded (b) annual, (c) winter and (d) summer SMB rates over the period 1960–2020 based on median parameter values. Glaciers with glaciological SMB records are highlighted (Sup: Supphellebreen, Tun: Tunsbergdalsbreen, Nig: Nigardsbreen, Aus: Austdalsbreen, Ves: Vesledalsbreen).

**Table 2.** Overview of modelled annual and seasonal SMB rates for Jostedalsgreen for different decades. Values in m w.e. a<sup>-1</sup> given as: rate (95% credible interval limits). Percentages are relative to median rate 1960–2020.

Period	Annual (m w.e. a <sup>-1</sup> )	Summer (m w.e. a <sup>-1</sup> )	Summer (%)	Winter (m w.e. a <sup>-1</sup> )	Winter (%)
1960–69	−0.60 (−0.76, −0.44)	−2.08 (−2.21, −1.95)	99%	1.48 (1.38, 1.56)	73%
1970–79	−0.22 (−0.38, −0.07)	−2.06 (−2.17, −1.93)	98%	1.82 (1.72, 1.93)	90%
1980–89	0.21 (0.06, 0.37)	−1.77 (−1.89, −1.66)	85%	1.98 (1.88, 2.12)	98%
1990–99	0.71 (0.56, 0.89)	−1.92 (−2.01, −1.82)	92%	2.63 (2.50, 2.78)	130%
2000–09	−0.37 (−0.54, −0.21)	−2.48 (−2.59, −2.37)	118%	2.09 (1.99, 2.23)	104%
2010–19	−0.29 (−0.46, −0.13)	−2.29 (−2.39, −2.18)	109%	1.99 (1.87, 2.11)	98%

341 respectively). However, within the past decade there are relatively large interannual variations in SMB,  
 342 with relatively high magnitudes both for positive and negative years (Fig. 4a).

343 Within the overall temporal trends there is significant variability in SMB between regions of the ice cap  
 344 (Figs. 5 and 6). We evaluate these trends on a decadal basis and for the regions North, Central, and South  
 345 (Fig. 1). The 1960s display negative annual SMB over most of the ice cap, with particularly negative rates  
 346 in the North (Fig. 6b). While the 1970s and 1980s indicate near balanced or positive rates for glaciers  
 347 in the South and Central parts, SMB rates in the North remain negative. In the 1990s, SMB rates are  
 348 overall positive for all three parts of the ice cap, with highest magnitude in the South. All regions display  
 349 negative SMB rates in the 2000s and 2010s. The South and Central parts show similar annual SMB rates  
 350 to the 1960s, but SMB rates for glaciers in the North parts are strikingly more negative in the 1960s and  
 351 70s compared to the 2000s.

352 Glaciers in the North and South of Jostedalsgreen generally display more negative summer SMB than  
 353 glaciers in the Central part (Fig. 6c). The largest winter SMB rates are generally found for glaciers in the  
 354 South of the ice cap (Figs. 5a and 6a). Magnitudes of summer SMB show considerable temporal variability  
 355 which is relatively uniform across regions (Fig. 6c). Differences in winter SMB, however, show both strong  
 356 temporal and spatial variability between decades, with particularly large variability in the North and South  
 357 (Fig. 6a).

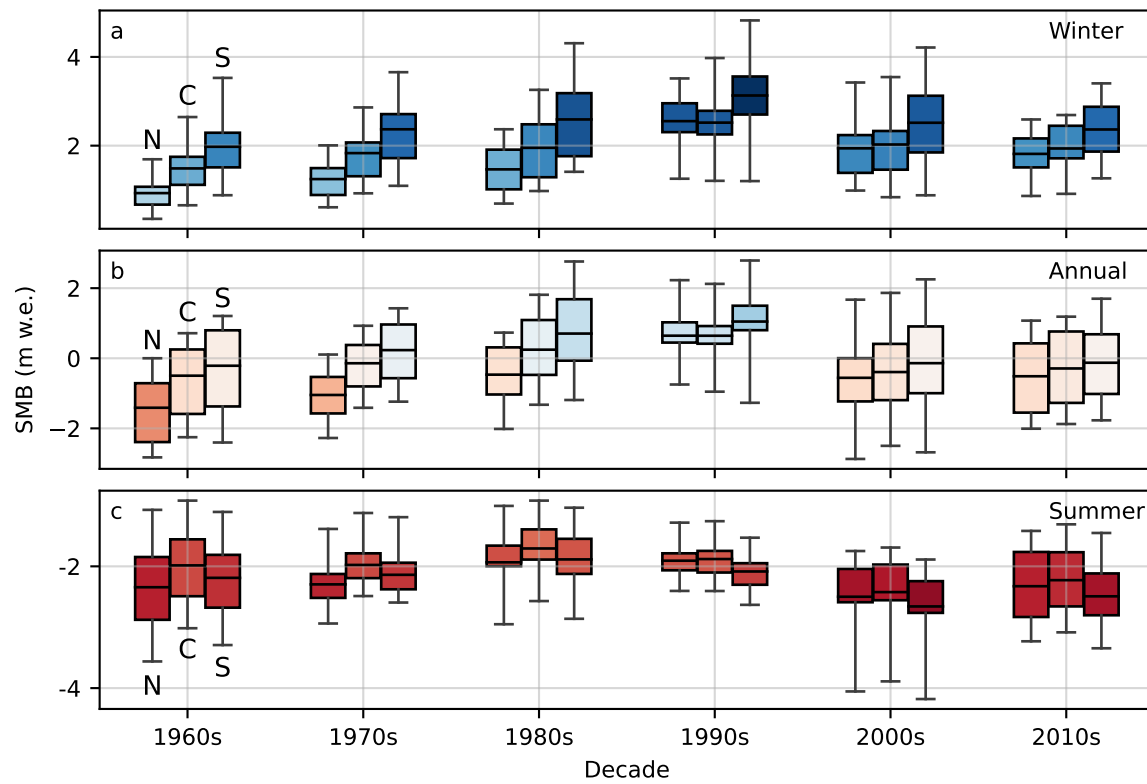


**Fig. 6.** Distribution of (a) winter, (b) annual and (c) summer surface mass balance (SMB; m w.e.) for different decades and regions in order: North (N), Central (C) and South (S). Horizontal lines in boxplots indicate SMB rate (mean) and boxes and whiskers extend to the interquartile range and minimum and maximum SMB, respectively.



## 358 5 DISCUSSION

### 359 5.1 Meteorological drivers of temporal variability in SMB

360 Our results indicate that temporal trends in SMB on Jostedalsbreen were largely driven by winter accu-  
361 mulation variability between 1960–2000, while increasingly negative summer ablation dominates annual  
362 SMB after 2000 (Table 2, Figs. 4 and 6). The mass gain during the late 1980s through the 1990s is  
363 in line with glaciological SMB records for Nigardsbreen and Austdalsbreen and subsequent advances of  
364 several outlet glaciers (e.g. Bergsetbreen, Bødalsbreen, Brenndalsbreen, Kjenndalsbreen, Nigardsbreen;  
365 NVE, 2022). This period of mass gain is found for glaciers in western Norway in general (e.g. Andreassen  
366 and others, 2005) and has been attributed to increased snow accumulation (Andreassen and others, 2005;  
367 Winkler and others, 2009) associated with transient changes in large scale weather patterns. In particu-  
368 lar, this period has been shown to coincide with a period of strongly positive North Atlantic Oscillation  
369 (NAO) index (e.g. Nesje and others, 2000; Marzeion and Nesje, 2012; Trachsel and Nesje, 2015; Mutz and  
370 others, 2016), which is characterized by strong westerly winds and anomalously high winter precipitation  
371 over western Scandinavia. The magnitude of our modelled 1990s winter SMB anomaly (Table 2) is also in  
372 line with weather station records which show that winter precipitation (December–February) in western  
373 Norway was particularly high in the 1990s (Hanssen-Bauer, 2005; Konstali and Sorteberg, 2022), up to 30%  
374 higher than the 1900–2019 mean in the mid 1990s (Konstali and Sorteberg, 2022). While regional trends in  
375 temperature do not indicate particularly low summer temperatures in the 1980s and 90s (Hanssen-Bauer,  
376 2005), our results indicate that lower magnitudes of ablation have contributed to the overall mass gain of  
377 Jostedalsbreen around the 1990s. In contrast to the 1990s, our findings suggest that mass losses of the ice  
378 cap in the 1960s were primarily driven by lower than average winter SMB. This anomaly is also supported  
379 by weather station records from western Norway that show a significant negative winter (Dec-Jan) precip-  
380 itation anomaly in the 1960s (around 25% lower than the 1900–2019 mean in the mid 1960s; Konstali and  
381 Sorteberg, 2022).

382 Our results indicate that increasingly negative summer balances are driving increased mass loss of  
383 Jostedalsbreen since the early 2000s (Table 2, Figs. 4 and 6), in line with previous findings for glaciers in  
384 Norway (e.g. Mutz and others, 2016). Overall, annual air temperature in western Norway has increased  
385 by around 0.7 °C from the start of the 20th century (1900–2014; Hanssen-Bauer and others, 2017) with  
386 the largest increases found in spring (March–May; 0.9 °C) and autumn (September–November; 0.8 °C).

387 The modelled mass loss of Jostedalsgreen from around 2000 is in line with the overall negative trends in  
388 glaciological SMB records in Norway, with the 2000s as the most negative decade (Andreassen and others,  
389 2020; Kjølmoen and others, 2022). Our results show that strongly negative summer SMB rates from the  
390 early 2000s are to some degree counteracted by relatively high winter SMB rates (Table 2 and Figs. 6a  
391 and c). Overall, precipitation in western Norway has increased by 18% between 1960 and 2019 (Konstali  
392 and Sorteberg, 2022), such that increased ablation due to higher temperatures may be compensated by  
393 increased winter accumulation. Andreassen and others (2020) found that the NAO-index was positive for  
394 several years in the 2010s, and attributed part of the overall less negative SMB of glaciers in Norway in this  
395 decade to high winter precipitation rates. We find that summer SMB at Jostedalsgreen was less negative  
396 in the 2010s compared to the 2000s (Table 2), but with relatively large interannual variations in both  
397 summer and winter SMB (Fig. 4a). This increases the sensitivity of our decadal analysis to partitioning  
398 of years. Considering the decade 2011–20 instead of 2010–19 gives a positive SMB rate of 0.14 m w.e. a<sup>-1</sup>  
399 (compared to -0.29 m w.e. a<sup>-1</sup> for 2010–19), with winter/summer SMB magnitudes 110/104% of the average  
400 of 1960–2020. Thus, controls on annual SMB in the 21st century seemingly vary between years. Large  
401 parts of Jostedalsgreen are located at high elevations; 72 (48)% of the area of the ice cap is located above  
402 1500 (1600) m.a.s.l. (2019 outline and DEM from 2020; the Norwegian Mapping Authority). This means  
403 that the ice cap currently has a relatively large accumulation area distributed over a small elevation range.  
404 However, with ongoing and future expected increases in temperatures and associated rising ELAs, as well  
405 as the feedback of surface lowering on SMB, it is unclear to what extent increased winter precipitation will  
406 continue to compensate for a shrinking accumulation area and stronger ablation.

407 Several studies (e.g. Nesje and others, 2000; Andreassen and others, 2005, 2020; Mernild and others,  
408 2014; Trachsel and Nesje, 2015) have investigated the influence of winter and summer SMB on annual  
409 SMB for glaciers in different climatic settings in Norway and found the same overall relationship: the  
410 annual SMB of maritime glaciers and continental glaciers is mainly controlled by winter precipitation and  
411 summer temperatures, respectively. Following the approach of Andreassen and others (2005, 2020), we  
412 compared ratios of the standard deviations in winter and summer SMB to standard deviations in annual  
413 SMB (sBw/sBa and sBs/sBa, respectively) for each glacier of Jostedalsgreen. When computing sBw/sBa  
414 and sBs/sBa over the time series as a whole, ratios are relatively equal (e.g. for Nigardsbreen sBw/sBa  
415 and sBs/sBa is 0.69 and 0.52, respectively) and in line with Andreassen and others (2005). However, when  
416 evaluating sBw/sBa and sBs/sBa over 20-year rolling windows, ratios are not stationary (e.g. between

417 0.57–0.86 for sBw/sBa and 0.37–0.60 for sBs/sBa for Nigardsbreen; Fig. D1). This analysis indicates  
418 that the relative contribution of winter SMB to annual SMB was particularly high towards the end of  
419 the 20th century but is decreasing towards the present, along with a simultaneous increase in the relative  
420 importance of summer SMB (Fig. D1). These findings are in line with Trachsel and Nesje (2015) who found  
421 that for Scandinavian (including Nigardsbreen), variations in winter precipitation was more important than  
422 variations in summer temperature for annual SMB in the second half of the 20th century, but that the  
423 relative influence of summer temperature has increased in more recent years.

## 424 5.2 Variability in SMB between glaciers and regions

425 Modelled glacier-wide SMB rates on Jostedalsbreen show spatially varying signals with some distinct re-  
426 gional patterns (Fig. 5): overall slightly positive SMB in the south, near balance in the central part (but  
427 with overall negative SMB for large outlet glaciers), and relatively large negative SMB in the north. Fol-  
428 lowing Andreassen and others (2023), we investigate topographic controls (statistics from 2019-inventory)  
429 on glacier-wide SMB rates over the period 1960–2020 and find the strongest correlation ( $-0.42$ ,  $p \leq 0.001$ )  
430 with hypsometric index (HI, calculated according to Jiskoot and others, 2009) and median elevation ( $0.39$ ,  
431  $p \leq 0.001$ ). The HI can be used to classify glaciers as very top heavy ( $HI < -1.5$ ), top heavy ( $-1.5 < HI < -$   
432  $1.2$ ), equidimensional ( $-1.2 < HI < 1.2$ ), bottom heavy ( $1.2 < HI < 1.5$ ) or very bottom heavy ( $HI > 1.5$ ).  
433 Our results indicate that glaciers with higher HI (more bottom heavy) or lower median elevation generally  
434 have more negative SMB rates. This is not unexpected since the hypsometry influences the relative size  
435 of the accumulation and ablation areas, and therefore glacier sensitivity to winter versus summer SMB.  
436 Andreassen and others (2023) found that median elevation showed the strongest correlation with geodetic  
437 mass balance for the smaller sample of 49 glaciers on central and northern Jostedalsbreen over the shorter  
438 period 1966–2020, but lower correlation for HI. It should be noted that we omitted the detached tongue of  
439 Brenndalsbreen (ID2301, categorized as very bottom heavy) from the correlation analysis since it should  
440 be considered as an outlier following the assumption of normality underlying the Pearson correlation co-  
441 efficient. We did not find strong correlations between annual SMB rates and other geometric variables  
442 (minimum elevation, maximum elevation, slope, aspect, length, area; the strongest of these is  $0.23$  for  
443 aspect,  $p \leq 0.05$ ).

444 To investigate potential topographical controls on regional patterns of SMB (Figs. 5 and 6), we consider  
445 the HI of glaciers in different regions of the ice cap (North, Central, and South; Fig. 1). Most bottom-heavy

446 glaciers (high HI) are located in the North region, consistent with the negative SMB rates found in this  
447 region. Meanwhile, nine of the 13 glaciers that can be characterized as equidimensional, bottom heavy  
448 or very bottom heavy, are located in North (e.g. Austdalsbreen and Vesledalsbreen), two are located in  
449 Central and two are located in South. However, glaciers in South generally have lower median elevations  
450 than glaciers in Central and North (98/69%, 85/50% and 63/11% of glaciers in Central, North and South,  
451 respectively, have median elevation >1500/1600 m a.s.l.). Lower median elevations in South and North  
452 compared to Central are in line with more negative summer SMB rates in these regions (Fig. 6c). However,  
453 topographic controls do not translate directly to regional patterns in annual SMB showing mostly balanced  
454 and positive SMB in South and negative SMB in North (Figs. 5 and 6b).

455 In addition to topographical controls, the regional differences in SMB on Jostedalsbreen can be explained  
456 by spatial variability in winter precipitation on the ice cap. For example, the South receives more winter  
457 precipitation than the rest of the ice cap, which drives high winter SMB in this region and compensates  
458 for relatively large negative summer SMB (Figs. 5c and 6). In addition, the North shows large temporal  
459 variability in winter SMB, with positive and negative anomalies of greater magnitude than the rest of  
460 the ice cap (55/152% of the 1960–2020 average in the 1960s/1990s). Jostedalsbreen is influenced by both  
461 frontal and orographic precipitation and precipitation amounts can show substantial local differences (e.g.  
462 Laute and Beylich, 2018). In this context it is interesting to note the magnitudes and spatial patterns  
463 of glacier-specific precipitation corrections (Fig. 3). Distributions of  $P_{corr,j}$  indicate that seNorge\_2018  
464 underestimates magnitudes of winter precipitation on Jostedalsbreen at different degrees, but particularly  
465 on the south-east facing and northern part of the ice cap. Due to the complex terrain around Jostedalsbreen,  
466 the ice cap's location in central western Norway and its large extent with a main ice divide stretching around  
467 60 km from south-west to north-east, it is likely that precipitation amounts are influenced by variations in  
468 weather patterns, as well as local topographical effects. In addition to the orographic effect on precipitation,  
469 redistribution of snow by wind may play a role. However, we expect the latter to be mainly relevant on a  
470 sub-grid scale, i.e. for the snow distribution across individual glacier units, but less important on a larger  
471 scale, when comparing individual glacier units or regions of the ice cap. Whether these combined effects  
472 are accurately captured in the meteorological dataset seNorge\_2018 is an open question that should be  
473 subject to further investigation.

### 474 5.3 Model performance

475 We evaluate model performance using data that is not employed in calibration of the model: glacier-wide  
476 SMB for odd years of glaciological SMB records, point SMB from stake measurements for all available  
477 years, and geodetic mass balance for parts of the ice cap (Andreassen and others, 2023). Details of the  
478 model performance evaluation can be found in Appendix C. Modelled SMB is generally in good agreement  
479 with glacier-wide and point SMB from glaciological records (Figs. C1 and C2). However, the comparison  
480 indicates that the magnitude of modelled ablation on the tongue of Nigardsbreen may be underestimated,  
481 but compensated by lower ablation at higher elevations such that modelled glacier-wide summer SMB  
482 agree well with glaciological records. This bias is supported by a slightly low value of the melt factor for  
483 ice compared to estimates from sonic ranger measurements on the tongue of Nigardsbreen in 2021 and  
484 2022 (Appendix C). However, this bias should not be overemphasized since the estimated melt factors  
485 only reflect conditions over a narrow time frame and geographical area, while model parameter values  
486 inherently reflect average conditions. Still, underestimation of ablation on glacier tongues could result in  
487 positive biases that are exacerbated with increasing temperatures.

488 Modelled SMB is also in agreement with geodetic mass balance of 49 glaciers (73% of the ice cap area)  
489 from 1966–2020 (Andreassen and others (2023); Fig. C3). Considering individual glaciers, the geodetic  
490 mass-balance rate is within 1.5 times the interquartile range of the modelled SMB rate for 34 of the  
491 49 glaciers. Spatial variability in modelled SMB is generally in agreement with geodetic mass balance,  
492 which shows most pronounced thinning in the north-east and on low-elevation glacier tongues (Andreassen  
493 and others, 2023). However, modelled glacier-wide SMB is more negative than geodetic mass balance for  
494 glaciers in the northern part of the ice cap (e.g. ID2471, ID2474 Vesledalsbreen, ID2478 Austdalsbreen,  
495 ID2481; Fig. C3). The glacier that shows the largest discrepancy is the detached tongue of Brenndalsbreen  
496 (ID2301), where the median modelled SMB rate is  $-3.66 \text{ m w.e.a}^{-1}$ , significantly more negative than the  
497 geodetic mass-balance rate of  $-0.54 \text{ m w.e.a}^{-1}$ . Brenndalsbreen is fed by ice falls and avalanches from  
498 above (Engen and others, 2024), processes which are not accounted for in the SMB model. Glaciers  
499 with large positive discrepancies between modelled surface and geodetic mass balance is the upper part  
500 of Brenndalsbreen (ID2305) and Briksdalsbreen (ID2316), both located in the central western part, and  
501 Bergsetbreen (ID2318) in the central-east. Other glaciers with large positive or negative discrepancies are  
502 smaller glaciers on the margins of the ice cap (e.g. IDs 2285; west, 2258 and 2489; north, 2328 and 2333;  
503 east). It should, however, be noted that the comparison (Fig. C3) does not account for the difference

504 in area used for calculating glacier-wide values (geodetic mass balance uses the average of the 1966 and  
505 2019 areas). In addition, geodetic mass balance estimates are converted from elevation to mass changes  
506 assuming a constant density, which may not reflect the spatial variability in snow, firn and ice densities  
507 across the ice cap.

508 It is important to mention that our model employs the seNorge\_2018 DEM for the entire period 1960–  
509 2020, such that surface elevation changes are not accounted for. However, we consider the effect of surface  
510 lowering on mass balance to be negligible since surface elevation changes over Jostedalbreen are limited  
511 over this period (Andreassen and others, 2023). The overall change in ice cap area over the modelling  
512 period is also relatively small, with a reduction of 5.2% (26.0 km<sup>2</sup>) from 1966–2006 and 3.4% (15.9 km<sup>2</sup>)  
513 from 2006–19 (Andreassen and others, 2023). However, area changes vary between glaciers and periods,  
514 which means that for some glaciers modelled glacier-wide SMB estimates may be influenced by area changes  
515 not being properly accounted for.

#### 516 5.4 Spatiotemporal variations in model parameters

517 Our obtained precipitation correction factors suggests that precipitation sums in seNorge\_2018 are under-  
518 estimated. This is in line with previous results for glaciers along the maritime-continental climate gradient  
519 in southern Norway (Sjursen and others, 2023), and corroborated by comparison of modelled accumulation  
520 to distributed snow water equivalent derived using snow depth from ground-penetrating radar measure-  
521 ments on the ice cap (Fig. C4, see Appendix C for details). It is not uncommon that reanalysis datasets  
522 show variable performance in capturing precipitation in mountainous regions with complex terrain (e.g.  
523 Guidicelli and others, 2023; Zandler and others, 2019), and different versions of seNorge also show discrep-  
524 ancies in precipitation amounts (Lussana and others, 2019). However, since we simultaneously estimate  
525  $P_{corr,j}$  and  $T_{corr,j}$ , there are likely compensating effects of modelled ablation and accumulation on decadal  
526 SMB (Sjursen and others, 2023), such that care should be taken when interpreting the magnitude of bi-  
527 ases. Nevertheless, the posterior of  $P_{corr,j}$  is unlikely to deviate strongly from its well-constrained prior  
528 ( $P_{corr,glob}$ ). The advantage of this is that  $P_{corr,j}$  is informed by measurements of winter accumulation  
529 (through  $P_{corr,glob}$ ). The disadvantage is that the spatial variability of  $P_{corr,j}$  will be somewhat limited. It  
530 should also be noted that parameter values are dependent on the values of fixed parameters, e.g. threshold  
531 temperature for snow likely affects magnitudes of  $P_{corr,j}$ , as well as other data used. Observations used for  
532 parameter estimation could be afflicted with biases, e.g. comparison of elevation differences from Hugonnet



533 and others (2021) with repeat LiDAR surveys for Nigardsbreen and Austdalsbreen indicates significantly  
534 more negative geodetic mass balance using repeat LiDAR (Andreassen and others, 2023). However, there  
535 are large differences in uncertainty between the two estimates, which presents an additional argument for  
536 accounting for uncertainty in observations used to constrain models as done in this study.

537 Since we employ constant melt factor distributions over the ice cap in step 2 of parameter estimation,  
538 spatial patterns in  $T_{corr,j}$  could also reflect spatial variations in melt factors, e.g. differences in solar  
539 radiation forcing between glaciers. If this was the case, we might expect more pronounced differences  
540 between predominantly north- or south-facing glaciers. Instead, variations in  $T_{corr}$  imply overall higher  
541 melt factors on the north-western compared to the south-eastern side of the ice cap. These differences  
542 could be explained by limitations in seNorge\_2018, unresolved processes in the model and/or compensating  
543 effects of ablation and accumulation on decadal SMB. Nevertheless, constant melt factor distributions are  
544 a limitation of our model set-up, as melt factors have been shown to be transient (e.g. Gabbi and others,  
545 2014; Ismail and others, 2023). However, we expect this temporal variability to at least partly be reflected  
546 in posterior distributions.

547 In relation to spatiotemporal variations in melt factors, it is interesting to compare the posterior es-  
548 timate of  $MF_{snow}$  to values from Sjursen and others (2023), where posterior distributions of  $MF_{snow}$   
549 were estimated for Nigardsbreen and Austdalsbreen individually, using seasonal glaciological SMB over  
550 the period 2000–2019. Compared to this study their estimates are slightly lower for Austdalsbreen  
551 ( $3.53/3.51 \pm 0.28$  mm w.e.  $^{\circ}\text{C}^{-1}\text{d}^{-1}$ ) and somewhat higher for Nigardsbreen ( $4.21/4.21 \pm 0.42$  mm w.e.  $^{\circ}\text{C}^{-1}\text{d}^{-1}$ ),  
552 and with somewhat higher uncertainty (likely due to the combination of a larger set of observations and  
553 compensation by the model error estimated in this study). Melt factors are expected to decrease with an  
554 earlier onset of melt (Ismail and others, 2023), which may be occurring at Jostedalsbreen with the increase  
555 in spring temperatures over the past century (Hanssen-Bauer and others, 2017). However, comparison to  
556 melt factors for the recent period 2000–2019 do not indicate this. The difference between the estimates  
557 likely reflects both spatial and temporal variability, since melt factors in this study reflect variability over a  
558 longer time period and a spatial compromise between five glaciers. In addition, since posterior distributions  
559 here are jointly estimated (e.g. with  $T_{corr}$ ), comparison of parameter values for individual glaciers should  
560 not be overemphasized.

561 Encompassing possible spatiotemporal variations in parameter uncertainty and model error high-  
562 lights our argument for performing rigorous uncertainty estimation in SMB modelling, particularly in

563 temperature-index models where melt processes are parameterized. This is particularly important since  
564 it is unclear if temperature-index models with constant parameter values are suitable for modelling SMB  
565 under changing climatic conditions, with studies showing contradicting evidence (e.g Gabbi and others,  
566 2014; Réveillet and others, 2018; Ismail and others, 2023). Energy-balance approaches have the advantage  
567 of constraining and explaining underlying physical processes. Increased availability of high-resolution cli-  
568 mate products will alleviate their reliance on in-situ meteorological data and/or downscaling of relatively  
569 coarse-resolution climate model input to the scale of the glacier. However, energy-balance models will  
570 still rely on site-specific assessment of a parameter space with significant model sensitivity (e.g. Zolles  
571 and others, 2019) that is currently more difficult to explore due to computational demands. Although  
572 the method demonstrated here may be more readily applied with temperature-index approaches due to  
573 their lower computational cost, novel methodological developments, e.g. approximate Bayesian inference  
574 by using emulators to explore the relationship between parameters and observations (Cleary and others,  
575 2021), could provide similar opportunities with more computationally expensive models.

576 Our parameter estimation set-up is similar to the empirical Bayesian approach of Rounce and others  
577 (2020a,b, 2023), where regional prior distributions are first estimated empirically by aggregating optimized  
578 parameter values for each glacier in a region, followed by estimation of a posterior parameter distribution for  
579 each individual glacier using satellite-derived geodetic mass balances in a Bayesian model. An important  
580 novelty in this study is that we also employ a Bayesian approach to estimate the prior distribution for  
581 the glacier-specific parameter estimation using seasonal glaciological SMB (step 1), such that the prior  
582 distribution in step 2 is well-constrained and represents plausible local magnitudes of accumulation and  
583 ablation. We recognize the possibility of adopting a full Bayesian hierarchical approach (see e.g. Gelman and  
584 others, 2014) where global and glacier-specific parameters could be estimated simultaneously by assuming  
585 that glacier-specific parameters are drawn from a common population. However, this would incur significant  
586 additional computational cost and it is unclear if it would provide any additional benefits in terms of  
587 constraining model parameters and modelled SMB. Therefore, we believe that our two-step approach is  
588 sufficient in this respect and provides additional flexibility in terms of interpreting both global and glacier-  
589 specific parameter values.

590 With the increasing availability of satellite-borne datasets to inform SMB, we believe that SMB-  
591 modelling efforts should be adapted to take advantage of this new wealth of information to improve SMB  
592 estimates. We demonstrate one such method to leverage several observational datasets with complemen-

593 tary characteristics to provide robust spatiotemporal estimates of SMB over the relatively large and diverse  
594 region of Jostedalsbreen. Although seasonal glaciological SMB measurements to constrain accumulation  
595 and ablation, as used in this study, are not available in many regions of the world, it is likely that other  
596 datasets can be used to the same end, for example snow lines (e.g. Barandun and others, 2021; Geck and  
597 others, 2021) or higher resolution remote-sensing based glacier mass balance (e.g. Belart and others, 2017;  
598 Pelto and others, 2019; Falaschi and others, 2023).

## 599 6 CONCLUSION

600 We modelled the SMB of Jostedalsbreen ice cap in western Norway over the period 1960–2020 using a  
601 temperature-index model with assimilation of both seasonal glaciological SMB observations (available for  
602 five glaciers of the ice cap) and satellite remote-sensing based decadal geodetic mass balance for the entire  
603 Jostedalsbreen. This procedure allows us to constrain winter accumulation and summer ablation, while  
604 accounting for local differences between glaciers. Overall, we found that Jostedalsbreen was nearly in  
605 balance over the past 60 years, with a small annual average mass loss of  $-0.07$  m w.e.  $\text{a}^{-1}$  (95% CI: -  
606  $0.21$ ,  $0.08$  m w.e.  $\text{a}^{-1}$ ). In addition to large interannual variability in seasonal and annual SMB, the model  
607 reveals decadal trends in SMB that can be attributed to anomalies in winter accumulation and/or summer  
608 ablation. The 1960s were characterized by mass loss, mainly attributed to low winter accumulation. In  
609 contrast, the 1990s show significant mass gains driven by high winter accumulation. Finally, substantial  
610 mass loss occurred in the 2000s, dominated by increased summer ablation due to warming air temperatures.

611 Our results thus suggest that SMB trends on Jostedalsbreen in the second half of the 20th century have  
612 largely been driven by variations in winter SMB due to positive and negative winter precipitation anomalies.  
613 From the start of the 21st century SMB is dominated by increased ablation due to higher temperatures,  
614 but with interannual variability influenced by variations in winter precipitation, which partly offset the  
615 effects of warming in several recent years. The SMB evolution of Jostedalsbreen stands in contrast to  
616 overall global trends that show persistently negative SMB for most glaciers.

617 We find that SMB varies spatially between glaciers and regions. The northern part of the ice cap and  
618 low-lying glacier tongues display the most negative rates, while the southern part shows overall positive  
619 rates. Our model reveals that spatiotemporal variations in winter accumulation and summer ablation drive  
620 SMB patterns across Jostedalsbreen. These are linked to climate variability and ongoing climate change,  
621 on one hand, and local topographic controls, on the other hand. We expect such spatiotemporal differences

622 in SMB-controls to have a significant influence on the future evolution of the ice cap.

623 Our Bayesian approach demonstrates a framework for leveraging the advantages of different informa-  
624 tion sources: the constraints on parameter values offered by in-situ glaciological measurements and the  
625 unprecedented spatial coverage of satellite-derived geodetic observations that facilitate spatial adjustment  
626 of parameters to local conditions. The method allows for additional insights, such as revealing possible  
627 spatial biases in meteorological forcing data. Overall, parameter estimates indicate that winter precipita-  
628 tion in the seNorge\_2018 meteorological dataset is underestimated over Jostedalsbreen, although possibly  
629 at different degrees both spatially and temporally.

630 We highlight the need for accurate mass-balance observations with sufficient temporal resolution and  
631 spatial coverage in order to constrain mass balance models. Seasonal observations (such as provided by  
632 glaciological SMB measurements) allows the model to reproduce magnitudes of accumulation and ablation,  
633 while the spatial coverage offered by geodetic methods inform spatial variability. We therefore advocate  
634 employing complementary datasets that provide information about the spatiotemporal variability in glacier  
635 mass balance. The framework presented here illustrates an approach to utilize such datasets while simul-  
636 taneously addressing the inherent uncertainties in the observations to generate robust estimates of SMB.

## 637 DATA

638 The source code of the model is available in the GitHub repository [insert repository link]. seNorge\_2018 is  
639 available for download at [https://thredds.met.no/thredds/catalog/senorge/seNorge\\_2018/catalog.](https://thredds.met.no/thredds/catalog/senorge/seNorge_2018/catalog.html)  
640 [html](http://glacier.nve.no/glacier/viewer/ci/en/). Glaciological mass-balance observations can be found at [http://glacier.nve.no/glacier/viewer/](http://glacier.nve.no/glacier/viewer/ci/en/)  
641 [ci/en/](http://glacier.nve.no/glacier/viewer/ci/en/) and time series of glacier outlines for Nigardsbreen and Austdalsbreen are available in the model  
642 repository.

## 643 ACKNOWLEDGEMENTS

644 This work is a contribution to the JOSTICE project funded by the Norwegian Research Council (RCN  
645 grant #302458). We thank Hallgeir Elvehøy and Bjarne Kjølmoen (NVE) for providing mass-balance  
646 data and time series of glacier outlines for Nigardsbreen and Austdalsbreen and for valuable input on  
647 the results, and Kjetil Melvold (NVE) for providing snow depth estimates from ground-penetrating radar  
648 measurements on Jostedalsbreen. We would also like to thank HVL for providing computational resources  
649 to perform MCMC simulations.

650 **AUTHOR CONTRIBUTION**

651 KHS coded the mass-balance model, developed and coded the Bayesian parameter estimation routine,  
652 performed MCMC simulations and initial analysis, prepared figures and wrote the initial draft of the  
653 manuscript. TD and TVS provided input on parameter estimation. LMA provided homogenized glacier  
654 outlines for Jostedalsbreen and prepared Fig. 1. TD, TVS, LMA and HÅ all provided input to analysis of  
655 results and read and edited the manuscript.

656 **REFERENCES**

- 657 Andreassen LM and Oerlemans J (2009) Modelling long-term summer and winter balances and the climate  
658 sensitivity of Storbreen, Norway. *Geografiska Annaler: Series A, Physical Geography*, **91**(4), 233–251 (doi:  
659 10.1111/j.1468-0459.2009.00366.x)
- 660 Andreassen LM, Elvehøy H, Kjøllmoen B, Engeset R and Haakensen N (2005) Glacier mass-balance and length  
661 variation in Norway. *Annals of Glaciology*, **42**, 317–325 (doi: 10.3189/172756405781812826)
- 662 Andreassen LM, Winsvold S, Paul F and Hausberg J (2012) Inventory of norwegian glaciers. Technical report,  
663 Norwegian Water Resources and Energy Directorate (doi: 10.5167/uzh-73855)
- 664 Andreassen LM, Elvehøy H, Kjøllmoen B and Engeset RV (2016) Reanalysis of long-term series of glaciological and  
665 geodetic mass balance for 10 Norwegian glaciers. *The Cryosphere*, **10** (doi: 10.5194/tc-10-535-2016)
- 666 Andreassen LM, Elvehøy H, Kjøllmoen B and Belart JM (2020) Glacier change in Norway since the 1960s – an  
667 overview of mass balance, area, length and surface elevation changes. *Journal of Glaciology*, **66**, 1–16 (doi: 10.  
668 1017/jog.2020.10)
- 669 Andreassen LM, Nagy T, Kjøllmoen B and Leigh JR (2022) An inventory of Norway’s glaciers and ice-marginal lakes  
670 from 2018-19 Sentinel-2 data. *Journal of Glaciology*, **68**(272), 1085–1106 (doi: 10.1017/jog.2022.20)
- 671 Andreassen LM, Robson BA, Sjursen KH, Elvehøy H, Kjøllmoen B and Carrivick JL (2023) Spatio-temporal vari-  
672 ability in geometry and geodetic mass balance of Jostedalsbreen ice cap, Norway. *Annals of Glaciology*, 1–18 (doi:  
673 10.1017/aog.2023.70)
- 674 Barandun M, Pohl E, Naegeli K, McNabb R, Huss M, Berthier E, Saks T and Hoelzle M (2021) Hot Spots of Glacier  
675 Mass Balance Variability in Central Asia. *Geophysical Research Letters*, **48**(11), 1–14 (doi: 10.1029/2020GL092084)

- 676 Belart JMC, Berthier E, Magnússon E, Anderson LS, Pálsson F, Thorsteinsson T, Howat IM, Aðalgeirsdóttir G,  
677 Jóhannesson T and Jarosch AH (2017) Winter mass balance of Drangajökull ice cap (NW Iceland) derived from  
678 satellite sub-meter stereo images. *The Cryosphere*, **11**(3), 1501–1517 (doi: 10.5194/tc-11-1501-2017)
- 679 Braithwaite RJ (2008) Temperature and precipitation climate at the equilibrium-line altitude of glaciers ex-  
680 pressed by the degree-day factor for melting snow. *Journal of Glaciology*, **54**(186), 437–444 (doi: 10.3189/  
681 002214308785836968)
- 682 Cleary E, Garbuno-Inigo A, Lan S, Schneider T and Stuart AM (2021) Calibrate, emulate, sample. *Journal of*  
683 *Computational Physics*, **424**(109716), 1–20, ISSN 0021-9991 (doi: 10.1016/j.jcp.2020.109716)
- 684 Cogley JG, Hock R, Rasmussen LA, Arendt AA, Bauder A, Braithwaite RJ, Jansson P, Kaser G, Möller M, Nicholson  
685 L and Zemp M (2011) Glossary of Glacier Mass Balance and Related Terms. Ihp-vii technical documents in  
686 hydrology no. 86, iacscontribution no. 2, UNESCO-IHP, Paris
- 687 Compagno L, Zekollari H, Huss M and Farinotti D (2021) Limited impact of climate forcing products on future  
688 glacier evolution in scandinavia and iceland. *Journal of Glaciology*, **67**(264), 727–743 (doi: 10.1017/jog.2021.24)
- 689 Cuffey KM and Paterson WSB (2010) *The Physics of Glaciers*. Elsevier, 4 edition, ISBN 978-0-12-369461-4
- 690 Dussailant I, Berthier E, Brun F, Masiokas M, Hugonnet R, Favier V, Rabatel A, Pitte P and Ruiz L (2019)  
691 Two decades of glacier mass loss along the Andes. *Nature Geoscience*, **12**(10), 802–808, ISSN 1752-0908 (doi:  
692 10.1038/s41561-019-0432-5)
- 693 Dyurgerov M and Meier M (1999) Analysis of winter and summer glacier mass balances. *Geografiska Annaler: Series*  
694 *A, Physical Geography*, **81**(4), 541–554 (doi: 10.1111/1468-0459.00082)
- 695 Eidhammer T, Booth A, Decker S, Li L, Barlage M, Gochis D, Rasmussen R, Melvold K, Nesje A and Sobolowski S  
696 (2021) Mass balance and hydrological modeling of the Hardangerjøkulen ice cap in south-central Norway. *Hydrology*  
697 *and Earth System Sciences*, **25**(8), 4275–4297 (doi: 10.5194/hess-25-4275-2021)
- 698 Engelhardt M, Schuler TV and Andreassen LM (2013) Glacier mass balance of Norway 1961-2010 calculated by a  
699 temperature-index model. *Annals of Glaciology*, **54**(63), 32–40, ISSN 0260-3055 (doi: 10.3189/2013AoG63A245)
- 700 Engelhardt M, Schuler TV and Andreassen LM (2014) Contribution of snow and glacier melt to discharge for  
701 highly glacierised catchments in Norway. *Hydrology and Earth System Sciences*, **18**(2), 511–523 (doi: 10.5194/  
702 hess-18-511-2014)
- 703 Engelhardt M, Schuler TV and Andreassen LM (2015) Sensitivities of glacier mass balance and runoff to climate  
704 perturbations in Norway. *Annals of Glaciology*, **56**(70), 79–88, ISSN 0260-3055 (doi: 10.3189/2015AoG70A004)



- 705 Engen SH, Gjerde M, Scheiber T, Seier G, Elvehøy H, Abermann J, Nesje A, Winkler S, Haualand KF, Rütther DC,  
706 Maschler A, Robson BA and Yde JC (2024) Investigation of the 2010 rock avalanche onto the regenerated glacier  
707 Brenndalsbreen, Norway. *Landslides*, 1–22, ISSN 1612-5118 (doi: 10.1007/s10346-024-02275-z)
- 708 Falaschi D, Bhattacharya A, Guillet G, Huang L, King O, Mukherjee K, Rastner P, Yao T and Bolch T (2023)  
709 Annual to seasonal glacier mass balance in High Mountain Asia derived from Pléiades stereo images: examples  
710 from the Pamir and the Tibetan Plateau. *The Cryosphere*, **17**(12), 5435–5458 (doi: 10.5194/tc-17-5435-2023)
- 711 Gabbi J, Carenzo M, Pellicciotti F, Bauder A and Funk M (2014) A comparison of empirical and physically based  
712 glacier surface melt models for long-term simulations of glacier response. *Journal of Glaciology*, **60**(224), 1140–1154  
713 (doi: 10.3189/2014JoG14J011)
- 714 Geck J, Hock R, Loso MG, Ostman J and Dial R (2021) Modeling the impacts of climate change on mass balance  
715 and discharge of Eklutna Glacier, Alaska, 1985–2019. *Journal of Glaciology*, **67**(265), 909–920 (doi: 10.1017/jog.  
716 2021.41)
- 717 Gelman A, Carlin JB, Stern HS, Dunson DB, Vehtari A and Rubin DB (2014) *Bayesian Data Analysis*. Chapman  
718 and Hall/CRC, Third edition, ISBN 978–1–4398–4095–5 (doi: 10.1201/b16018)
- 719 Giesen RH and Oerlemans J (2010) Response of the ice cap Hardangerjøkulen in southern Norway to the 20th and  
720 21st century climates. *The Cryosphere*, **4**(2), 191–213 (doi: 10.5194/tc-4-191-2010)
- 721 Gillespie MK, Andreassen LM, Huss M, de Villiers S, Sjursen KH, Aasen J, Bakke J, Cederstrøm JM, Elvehøy H,  
722 Kjølmoen B, Loe E, Meland M, Melvold K, Nerhus SD, Røthe TO, Støren ENW, Øst K and Yde JC (2024)  
723 Ice thickness and bed topography of Jostedalbreen ice cap, Norway. *Earth System Science Data Discussions*  
724 [preprint], 1–38 (doi: 10.5194/essd-2024-167), in review
- 725 Gjerde M, Hoel OL and Nesje A (2023) The ‘Little Ice Age’ advance of Nigardsbreen, Norway: A cross-disciplinary  
726 revision of the chronological framework. *The Holocene*, **33**(11), 1362–1375 (doi: 10.1177/09596836231185830)
- 727 Guidicelli M, Huss M, Gabella M and Salzmann N (2023) Spatio-temporal reconstruction of winter glacier mass  
728 balance in the Alps, Scandinavia, Central Asia and western Canada (1981–2019) using climate reanalyses and  
729 machine learning. *The Cryosphere*, **17**(2), 977–1002 (doi: 10.5194/tc-17-977-2023)
- 730 Haerberli W and Whiteman C (2021) Chapter 1 - Snow and ice-related hazards, risks, and disasters: Facing challenges  
731 of rapid change and long-term commitments. In W Haerberli and C Whiteman (eds.), *Snow and Ice-Related Hazards,*  
732 *Risks, and Disasters (Second Edition)*, Hazards and Disasters Series, 1–33, Elsevier, second edition edition, ISBN  
733 978-0-12-817129-5 (doi: 10.1016/B978-0-12-817129-5.00014-7)

- 734 Hanssen-Bauer I (2005) Regional temperature and precipitation series for Norway: Analyses of time-series updated  
735 to 2004. METreport 15/2005, The Norwegian Meteorological Institute (MET Norway), Oslo, Norway
- 736 Hanssen-Bauer I, Førland E, Haddeland I, Hisdal H, Mayer S, Nesje A, Nilsen J, Sandven SA, Sandø A, Sorteberg A  
737 and Ådlandsvi B (2017) Climate in Norway 2100. Norwegian Center for Climate Services (NCCS) Report 1/2017,  
738 Norwegian Environment Agency (Miljødirektoratet)
- 739 Hock R (2005) Glacier Melt: A Review of Processes and Their Modelling. *Progress in Physical Geography*, **29**(3)  
740 (doi: 10.1191/0309133305pp453ra)
- 741 Hugonnet R, McNabb R, Berthier E, Menounos B, Nuth C, Girod L, Farinotti D, Huss M, Dussailant I, Brun F and  
742 Kääb A (2021) Accelerated global glacier mass loss in the early twenty-first century. *Nature*, **592**(7856), 726–731,  
743 ISSN 1476-4687
- 744 Huss M and Hock R (2015) A new model for global glacier change and sea-level rise. *Frontiers in Earth Sciences*,  
745 **3**(54) (doi: 10.3389/feart.2015.00054)
- 746 Ismail MF, Bogacki W, Disse M, Schäfer M and Kirschbauer L (2023) Estimating degree-day factors of snow based  
747 on energy flux components. *The Cryosphere*, **17**(1), 211–231 (doi: 10.5194/tc-17-211-2023)
- 748 Jackson M and Ragulina G (2014) Inventory of glacier-related hazardous events in Norway. NVE Report 83/2014,  
749 Norwegian Water Resources and Energy Directorate (NVE) (doi: 10.13140/2.1.3462.0480)
- 750 Jennings KS, Winchell TS, Livneh B and Molotch NP (2018) Spatial variation of the rain–snow temperature threshold  
751 across the Northern Hemisphere. *Nature Communications*, **9**(1148), 1–9 (doi: 10.1038/s41467-018-03629-7)
- 752 Jiskoot H, Curran CJ, Tessler DL and Shenton LR (2009) Changes in Clemenceau Icefield and Chaba Group glaciers,  
753 Canada, related to hypsometry, tributary detachment, length–slope and area–aspect relations. *Annals of Glaciol-*  
754 *ogy*, **50**(53), 133–143 (doi: 10.3189/172756410790595796)
- 755 Kjøllmoen B (2017) Homogenisering av korte massebalanseserier i Norge. NVE Rapport no. 34/2020, Norwegian  
756 Water Resources and Energy Directorate, Oslo, Norway
- 757 Kjøllmoen B (2022) Reanalysing a glacier mass balance measurement series - Nigardsbreen 2014–2020. Nve rapport  
758 no. 7/2022, Norwegian Water Resources and Energy Directorate, Oslo, Norway
- 759 Kjøllmoen B, Andreassen LM, Elvehøy H and Storheil S (2022) Glaciological investigations in Norway. NVE Rapport  
760 no. 27/2022, Norwegian Water Resources and Energy Directorate, Oslo, Norway
- 761 Konstali K and Sorteberg A (2022) Why has Precipitation Increased in the Last 120 Years in Norway? *Journal of*  
762 *Geophysical Research: Atmospheres*, **127**(15), 1–18 (doi: 10.1029/2021JD036234)

- 763 Kumar R, Carroll C, Hartikainen A and Martin O (2019) ArviZ a unified library for exploratory analysis of Bayesian  
764 models in Python. *Journal of Open Source Software*, **4**(33), 1143 (doi: 10.21105/joss.01143)
- 765 Laumann T and Nesje A (2009) The impact of climate change on future frontal variations of Briksdalsbreen, western  
766 Norway. *Journal of Glaciology*, **55**(193), 789–796 (doi: 10.3189/002214309790152366)
- 767 Laute K and Beylich AA (2018) Potential effects of climate change on future snow avalanche activity in western  
768 Norway deduced from meteorological data. *Geografiska Annaler: Series A, Physical Geography*, **100**(2), 163–184  
769 (doi: 10.1080/04353676.2018.1425622)
- 770 Li H, Beldring S, Xu CY, Huss M, Melvold K and Jain SK (2015) Integrating a glacier retreat model into a hydrological  
771 model – Case studies of three glacierised catchments in Norway and Himalayan region. *Journal of Hydrology*, **527**,  
772 656–667, ISSN 0022-1694 (doi: 10.1016/j.jhydrol.2015.05.017)
- 773 Lussana C (2020) seNorge observational gridded dataset. seNorge\_2018, version 20.05. METreport 07/2020, The  
774 Norwegian Meteorological Institute (MET Norway), Oslo, Norway
- 775 Lussana C (2021) seNorge observational gridded datasets, seNorge\_2018, versions 21.09 and 21.10. METreport  
776 07/2021, The Norwegian Meteorological Institute (MET Norway), Oslo, Norway
- 777 Lussana C, Tveito O, Dobler A and Tunheim K (2019) seNorge\_2018, daily precipitation, and temperature datasets  
778 over Norway. *Earth System Science Data*, **11**(4), 1531–1551, ISSN 1866-3516 (doi: 10.5194/essd-11-1531-2019)
- 779 Marzeion B and Nesje A (2012) Spatial patterns of North Atlantic Oscillation influence on mass balance variability  
780 of European glaciers. *The Cryosphere*, **6**(3), 661–673 (doi: 10.5194/tc-6-661-2012)
- 781 Mernild SH, Hanna E, Yde JC, Seidenkrantz MS, Wilson R and Knudsen NT (2014) Atmospheric and oceanic  
782 influence on mass balance of northern North Atlantic region land-terminating glaciers. *Geografiska Annaler: Series*  
783 *A, Physical Geography*, **96**(4), 561–577 (doi: 10.1111/geoa.12053)
- 784 Mohr M (2008) New Routines for Gridding of Temperature and Precipitation Observations for “seNorge. no”. Tech-  
785 nical Report 08/2008, Norwegian Meteorological Institute, Oslo, Norway
- 786 Mutz S, Paeth H and Winkler S (2016) Modelling of future mass balance changes of Norwegian glaciers by ap-  
787 plication of a dynamical-statistical model. *Climate Dynamics*, **46**(5), 1581–1597, ISSN 1432-0894 (doi: 10.1007/  
788 s00382-015-2663-5)
- 789 Nesje A (2023) Future state of Norwegian glaciers: Estimating glacier mass balance and equilibrium line responses  
790 to projected 21st century climate change. *The Holocene*, **0**(0), 1–15 (doi: 10.1177/09596836231183069)

- 791 Nesje A, Lie Ø and Dahl SO (2000) Is the North Atlantic Oscillation reflected in Scandinavian glacier mass  
792 balance records? *Journal of Quaternary Science*, **15**(6), 587–601 (doi: 10.1002/1099-1417(200009)15:6<587::  
793 AID-JQS533>3.0.CO;2-2)
- 794 Nesje A, Bakke J, Dahl SO, Lie Ø and Matthews JA (2008) Norwegian mountain glaciers in the past, present and  
795 future. *Global and Planetary Change*, **60**(1), 10–27, ISSN 0921-8181 (doi: 10.1016/j.gloplacha.2006.08.004)
- 796 NVE (2022) Climate indicator products. <http://glacier.nve.no/viewer/CI/>, Norwegian Water Resources and Energy  
797 Directorate, Oslo, Norway
- 798 Oerlemans J (1992) Climate sensitivity of glaciers in southern Norway: application of an energy-balance model  
799 to Nigardsbreen, Hellstugubreen and Alftobreen. *Journal of Glaciology*, **38**(129), 223–232 (doi: 10.3189/  
800 S0022143000003634)
- 801 Oerlemans J (1997) A flowline model for Nigardsbreen, Norway: projection of future glacier length based on dynamic  
802 calibration with the historic record. *Annals of Glaciology*, **24**, 382–389 (doi: 10.3189/S0260305500012489)
- 803 Østrem G, Liestøl O and Wold B (1976) Glaciological investigations at Nigardsbreen, Norway. *Norsk Geografisk*  
804 *Tidsskrift - Norwegian Journal of Geography*, **30**(4), 187–209 (doi: 10.1080/00291957608552005)
- 805 Pelto BM, Menounos B and Marshall SJ (2019) Multi-year evaluation of airborne geodetic surveys to estimate  
806 seasonal mass balance, Columbia and Rocky Mountains, Canada. *The Cryosphere*, **13**(6), 1709–1727 (doi: 10.  
807 5194/tc-13-1709-2019)
- 808 Réveillet M, Vincent C, Six D and Rabatel A (2017) Which empirical model is best suited to simulate glacier mass  
809 balances? *Journal of Glaciology*, **63**(237), 39–54 (doi: 10.1017/jog.2016.110)
- 810 Réveillet M, Six D, Vincent C, Rabatel A, Dumont M, Lafaysse M, Morin S, Vionnet V and Litt M (2018) Relative  
811 performance of empirical and physical models in assessing the seasonal and annual glacier surface mass balance of  
812 Saint-Sorlin Glacier (French Alps). *The Cryosphere*, **12**(4), 1367–1386 (doi: 10.5194/tc-12-1367-2018)
- 813 Rounce DR, Hock R and Shean DE (2020a) Glacier Mass Change in High Mountain Asia Through 2100 Using the  
814 Open-Source Python Glacier Evolution Model (PyGEM). *Frontiers in Earth Science*, **7**, 331, ISSN 2296-6463 (doi:  
815 10.3389/feart.2019.00331)
- 816 Rounce DR, Khurana T, Short MB, Hock R, Shean DE and Brinkerhoff DJ (2020b) Quantifying parameter un-  
817 certainty in a large-scale glacier evolution model using Bayesian inference: application to High Mountain Asia.  
818 *Journal of Glaciology*, 1–13 (doi: 10.1017/jog.2019.91)

- 819 Rounce DR, Hock R, Maussion F, Hugonnet R, Kochtitzky W, Huss M, Berthier E, Brinkerhoff D, Compagno L,  
820 Copland L, Farinotti D, Menounos B and McNabb RW (2023) Global glacier change in the 21st century: Every  
821 increase in temperature matters. *Science*, **379**(6627), 78–83 (doi: 10.1126/science.abo1324)
- 822 Salvatier J, Wiecki TV and Fonnesbeck C (2016) Probabilistic programming in Python using PyMC3. *PeerJ Computer  
823 Science*, **2**(e55) (doi: <https://doi.org/10.7717/peerj-cs.55>)
- 824 Schuler T, Hock R, Jackson M, Elvehøy H, Braun M, Brown I and Hagen J (2005) Distributed mass balance modelling  
825 on Engabreen (Norway). *Annals of Glaciology*, **42**, 395–401 (doi: 10.3189/172756405781812998)
- 826 Schuster L, Rounce DR and Maussion F (2023) Glacier projections sensitivity to temperature-index model choices  
827 and calibration strategies. *Annals of Glaciology*, 1–16 (doi: 10.1017/aog.2023.57)
- 828 Shean DE, Bhushan S, Montesano P, Rounce DR, Arendt A and Osmanoglu B (2020) A Systematic, Regional  
829 Assessment of High Mountain Asia Glacier Mass Balance. *Frontiers in Earth Science*, **7**, 363, ISSN 2296-6463 (doi:  
830 10.3389/feart.2019.00363)
- 831 Singh P, Kumar N and Arora M (2000) Degree-day factors for snow and ice for Dokriani Glacier, Garhwal Himalayas.  
832 *Journal of Hydrology*, **235**(1), 1–11, ISSN 0022-1694 (doi: [https://doi.org/10.1016/S0022-1694\(00\)00249-3](https://doi.org/10.1016/S0022-1694(00)00249-3))
- 833 Sjursen KH, Dunse T, Tambue A, Schuler TV and Andreassen LM (2023) Bayesian parameter estimation in glacier  
834 mass-balance modelling using observations with distinct temporal resolutions and uncertainties. *Journal of Glaciol-  
835 ogy*, 1–20 (doi: 10.1017/jog.2023.62)
- 836 Trachsel M and Nesje A (2015) Modelling annual mass balances of eight Scandinavian glaciers using statistical  
837 models. *The Cryosphere*, **9**(4), 1401–1414 (doi: 10.5194/tc-9-1401-2015)
- 838 Vehtari A, Gelman A, Simpson D, Carpenter B and Bürkner PC (2021) Rank-Normalization, Folding, and Localiza-  
839 tion: An Improved  $\hat{R}$  for Assessing Convergence of MCMC (with Discussion). *Bayesian Analysis*, **16**(2), 667–718  
840 (doi: 10.1214/20-BA1221)
- 841 WGMS (2024) *Fluctuations of Glaciers Database*. World Glacier Monitoring Service (WGMS), Zurich, Switzerland  
842 (doi: 10.5904/wgms-fog-2024-01)
- 843 Winkler S (1996) Front variations of outlet glaciers from Jostedalbreen, western Norway, during the twentieth  
844 century. *Norges Geologiske Undersøkelse Bulletin*, **431**, 33–47
- 845 Winkler S, Elvehøy H and Nesje A (2009) Glacier fluctuations of Jostedalbreen, western Norway, during the past  
846 20 years: the sensitive response of maritime mountain glaciers. *The Holocene*, **19**(3), 395–414 (doi: 10.1177/  
847 0959683608101390)

- 848 Winsvold SH, Andreassen LM and Kienholz C (2014) Glacier area and length changes in Norway from repeat  
849 inventories. *The Cryosphere*, **8**(5), 1885–1903 (doi: 10.5194/tc-8-1885-2014)
- 850 Wong WK, Haddeland I, Lawrence D and Beldring S (2016) Gridded 1 x 1 km climate and hydrological projections  
851 for Norway. NVE report 59/2016, Norwegian Water Resources and Energy Directorate (NVE), Oslo, Norway
- 852 Zandler H, Haag I and Samimi C (2019) Evaluation needs and temporal performance differences of gridded pre-  
853 cipitation products in peripheral mountain regions. *Scientific Reports*, **9**(15118), 1–15, ISSN 2045-2322 (doi:  
854 10.1038/s41598-019-51666-z)
- 855 Zekollari H, Huss M, Farinotti D and Lhermitte S (2022) Ice-Dynamical Glacier Evolution Modeling - A Review.  
856 *Reviews of Geophysics*, **60**(2), 1–65 (doi: 10.1029/2021RG000754)
- 857 Zemp M, Thibert E, Huss M, Stumm D, Rolstad Denby C, Nuth C, Nussbaumer SU, Moholdt G, Mercer A, Mayer  
858 C, Joerg PC, Jansson P, Hynek B, Fischer A, Escher-Vetter H, Elvehøy H and Andreassen LM (2013) Reanalysing  
859 glacier mass balance measurement series. *The Cryosphere*, **7**(4), 1227–1245 (doi: 10.5194/tc-7-1227-2013)
- 860 Zolles T, Maussion F, Galos SP, Gurgiser W and Nicholson L (2019) Robust uncertainty assessment of the spatio-  
861 temporal transferability of glacier mass and energy balance models. *The Cryosphere*, **13**(2), 469–489, ISSN 1994-  
862 0424 (doi: 10.5194/tc-13-469-2019)

## 863 APPENDIX

### 864 APPENDIX A - LIST OF GLACIER IDS FOR EACH REGION

865 We provide a list of NVE glacier IDs part of each region of Jostedalsgreen (North, Central, and South,  
866 Fig. 1). Glacier IDs considered part of Jostedalsgreen in 1966, 2012, and 2019 inventories are in normal  
867 font. Glacier IDs only considered part of the ice cap in 1966 and 2012 inventories (82 in total) are marked  
868 in *italic* font, while IDs part of the ice cap only in the 2019 inventory (81 in total) are marked in **bold** font.

869 South: 2338, 2341, 2342, 2347, 2344, 2340, 2343, 2348, 2349, 2352, 2355, 2358, 2354, 2360, 2361, 2362,  
870 2364, *2367, 2369*

871 Central: 2250, 2266, 2258, 2246, 2271, 2283, 2265, 2255, 2273, 2289, 2280, 2297, 2299, 2311, 2308, 2309,  
872 2296, 2318, 2326, 2320, 2305, 2301, 2294, 2291, 2284, 2285, 2281, 2316, 2327, 2328, 2333, 2339, 2322,  
873 2324, 2325, 2323, 2319, 2321, 2329, 2331, 2334, 2336, 2332, **6762**

874 North: 2481, 2486, 2487, 2489, 2480, 2478, 2485, 2474, 2471, 2476, 2461, 2457, 2453, 2465, 2451, 2463,  
875 2459, 2468, 2488, 2490

## 876 **APPENDIX B - MARKOV CHAIN MONTE CARLO (MCMC) SIMULATIONS**

877 We use Markov chain Monte Carlo (MCMC) simulations to approximate posterior probability distribu-  
878 tions of  $\theta$ ,  $\sigma_\eta$ , and  $\phi_j$  following Sjursen and others (2023). The Bayesian framework is set up with the  
879 PyMC3 Python package (Salvatier and others, 2016), and MCMC simulations are performed using the  
880 DEMetropolisZ algorithm with four chains with 2000 tune and 10000/4000 sampling iterations in each  
881 chain for step 1/2 of the parameter estimation procedure. Convergence of MCMC simulations is assessed  
882 using visual and numerical convergence diagnostics recommended by Vehtari and others (2021) and avail-  
883 able tools in the ArviZ Python package (Kumar and others, 2019): the effective sample size for the bulk  
884 and tail of the distributions (ESS), the rank-normalized  $\hat{R}$  diagnostic, and the Monte Carlo Standard Error  
885 (MCSE) of posterior estimators (i.e. error in the expected value of the mean and standard deviation). Trace  
886 and density plots show good mixing of chains and consistent marginal posterior densities across chains,  
887 indicating that the posteriors are stationary and sufficiently explored. The minimum ESS (bulk/tail) is  
888 1118/1475 and 1811/1912 for marginal posterior distributions in step 1 and step 2, respectively, well above  
889 the recommended threshold of 400 (Vehtari and others, 2021). The rank-normalized  $\hat{R}$  metric is below  
890 1.01 for all simulations, indicating that there are no convergence issues. MCSE for the mean and standard  
891 deviation are less than 0.01 for all posterior estimates, which we consider to be sufficient precision. We  
892 are thus confident that our MCMC simulations provide adequate approximations of the marginal posterior  
893 distributions for all parameters.

## 894 **APPENDIX C - MODEL PERFORMANCE EVALUATION**

895 We validate modelled SMB using three sets of mass-balance observations: 1) glacier-wide glaciological  
896 SMB based on in-situ observations at mass-balance stakes (Table 1) for mass-balance years not employed  
897 in estimation of the global parameter set (odd years of the records; Fig. C1a), 2) point SMB from all  
898 individual stake measurements (Fig. C1b and c, data not available for Supphellebreen), and 3) geodetic  
899 mass balance for 49 of 82 glaciers (73% of total ice cap area) over the period 1966–2020 (Andreassen and  
900 others (2023); Fig. C3). In addition, we compare estimated  $MF_{ice, glob} = MF_{snow, glob}/0.7$  to melt factors for  
901 ice derived from daily melt rates from a sonic ranger on the tongue of Nigardsbreen in summer of 2021 and



902 2022, and modelled snow accumulation in 2020/2021 to estimated snow depth from ground-penetrating  
903 radar measurements collected over parts of the ice cap in April 2021 (Fig C4).

904 Comparison of modelled SMB to glacier-wide glaciological SMB shows overall low bias in modelled  
905 seasonal and annual SMB (Fig. C1a). Root mean squared error (RMSE) is lowest for winter and summer  
906 SMB, which is not surprising since the global parameter set was estimated using seasonal observations.  
907 The smallest biases are found for Nigardsbreen, Austdalsbreen and Tunsbergdalsbreen. Vesledalsbreen  
908 and Tunsbergdalsbreen show relatively large negative biases both for annual, summer and winter SMB,  
909 but results are only based of glaciological SMB from three mass-balance years. The average uncertainties  
910 (standard deviation of 1000 posterior predictive samples) in modelled glacier-wide annual, summer and  
911 winter SMB is 0.58 m w.e., 0.38 m w.e. and 0.43 m w.e. which is in the range of the mean absolute  
912 error (MAE) between modelled and observed glacier-wide annual (0.65 m w.e.), summer (0.35 m w.e.) and  
913 winter (0.39 m w.e.) SMB. We also visualize the time series of modelled SMB over the period of available  
914 glaciological glacier-wide SMB observations for the glaciers with the two longest records (Nigardsbreen  
915 and Austdalsbreen; Fig. C2). Overall, modelled SMB shows good correspondence with glaciological SMB  
916 records, but with some biases over certain time periods, e.g. modelled annual SMB for Nigardsbreen is  
917 somewhat higher than observations in the 1980s as a result of a positive bias in modelled summer SMB  
918 during this period (Fig. C2a and b), and annual SMB may be overestimated for Austdalsbreen in the 1990s  
919 due to a positive bias in modelled winter SMB (Fig. C2c and d).

920 Modelled annual SMB and stake measurements shows good agreement (Fig. C1b), in particular con-  
921 sidering the wide range of values. Magnitudes of summer and winter SMB (Fig. C1c) are generally slightly  
922 underestimated by the model. Biases are mostly related to very positive winter and negative summer  
923 SMB. Since the point SMB comparison is performed on the 1 km model grid (nearest-neighbour to stake  
924 location), some discrepancies should be expected due to unresolved topography, especially in steeper parts  
925 where the elevation of the grid cell may not be representative of the stake elevation. This may be a con-  
926 tributing factor to the positive bias in very negative summer SMB from stakes on the low-lying tongue  
927 of Nigardsbreen which is situated in a narrow valley. It should also be noted that glacier-wide and stake  
928 SMB comparisons are biased towards Nigardsbreen, which accounts for 29 of a total of 53 seasonal and 57  
929 annual glacier-wide SMB observations and 78% of stake measurements. The very negative summer point  
930 SMB from stakes on the tongue of Nigardsbreen (summer SMB measurements <-5 m w.e. have a mean  
931 elevation of 580 m a.s.l.; 227 points) is not representative of most of the area of the ice cap.

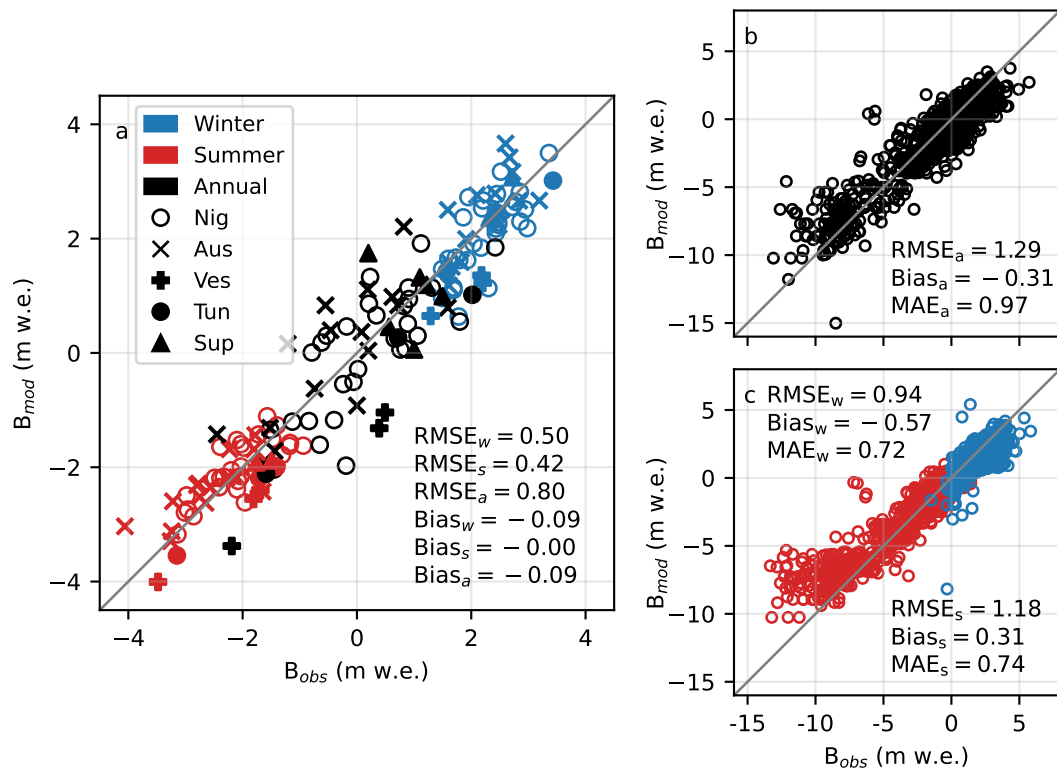


**Fig. C1.** (a) Median of posterior predictive distributions of glacier-wide summer, winter and annual surface mass balance (SMB) versus glaciological SMB in validation years (odd years 1963–2019, five glaciers; Nig: Nigardsbreen, Aus: Austdalsbreen, Ves: Vesledalsbreen, Tun: Tunsbergdalsbreen, and Sup: Supphellebreen). Modelled vs. measured (b) annual and (c) summer and winter point SMB over the period 1962–2020 for four glaciers with available stake measurements (Nig; 952/988/891 annual/summer/winter points, Aus; 89/89/89, Ves; 89/106/89, Tun; 71/84/71). Modelled point SMB is retrieved using median parameter values and for the dates and locations of each stake measurement. Units of root mean squared error (RMSE), bias and mean absolute error (MAE) are m w.e.

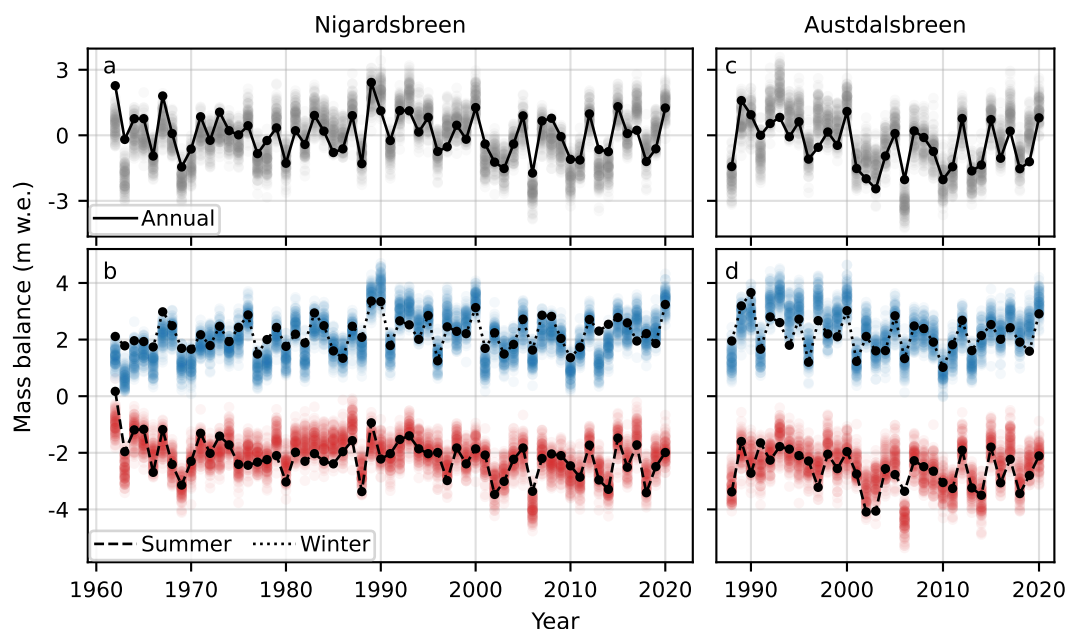


**Fig. C2.** Time series of posterior predictive (100 samples) annual and seasonal glacier-wide surface mass balance (SMB) for Nigardsbreen (a and b, respectively) and Austdalsbreen (c and d, respectively) over the periods of available glaciological SMB measurements (1962–2020 and 1988–2020, respectively). Posterior predictive samples of modelled annual, summer and winter SMB are shown as grey, red and blue circles, respectively. Glaciological SMB measurements are shown as black dots connected by solid, dashed and dotted lines for annual, summer and winter SMB, respectively.

932 The geodetic mass balance of an area covering 49 glaciers of Jostedalbreen (central and northern parts)  
 933 over the period 1966–2020 was estimated to  $-0.15 \pm 0.02$  m w.e.a<sup>-1</sup> (Andreassen and others, 2023). The  
 934 median modelled SMB rate of these 49 glaciers over the mass-balance years 1967–2020 is  $-0.06$  m w.e.a<sup>-1</sup>  
 935 (95% CI:  $-0.17, 0.04$  m w.e.a<sup>-1</sup>). Our estimated SMB rate differs slightly from the geodetic mass-balance  
 936 rate, which is not surprising given the inherent differences between the methods and that the geodetic  
 937 mass-balance also accounts for internal and basal accumulation and ablation (Zemp and others, 2013).  
 938 Of these sources, internal and basal ablation due to dissipative melting are considered non-negligible for  
 939 glaciers on the Norwegian mainland (Andreassen and others, 2016). The estimated mean rate of internal  
 940 and basal ablation over the 49 glaciers is  $-0.07$  m w.e a<sup>-1</sup> over the period 1966–2020 (Andreassen and  
 941 others, 2023). Taking this estimate into account, the modelled SMB for the 49 glaciers over the period  
 942 1966/67–2019/20 is in good agreement with the geodetic mass balance.

943 We estimate melt factors for ice for the summer season of 2021 (81 values over the period 2 July to 30  
 944 Sept) and 2022 (62 values over the period 17 July to 20 Sept) using daily surface height difference from  
 945 a sonic ranger and temperature from a weather station at approximately 600 m a.s.l. on the tongue of

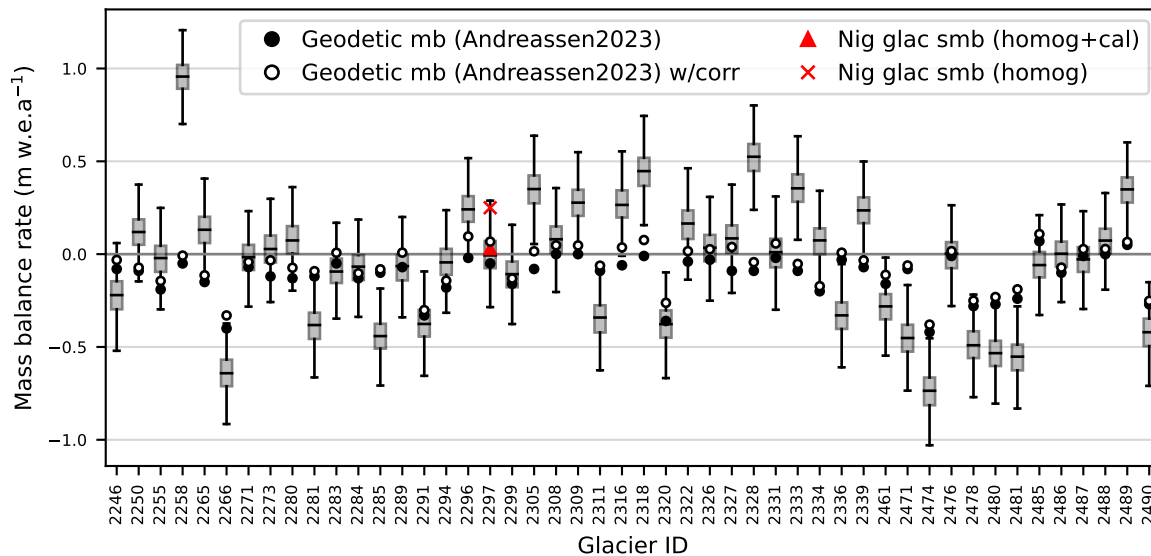


**Fig. C3.** Modelled glacier-wide surface mass-balance (SMB) rate over mass-balance years 1967–2020 for 48 glaciers of Jostedalbreen (box plots) with geodetic mass-balance estimates for 1966–2020 (points; Andreassen and others (2023)). Black horizontal lines in boxplots show medians, grey shaded areas show interquartile range (IQR; Q1–Q3) and whiskers extend to 1.5 IQR. Black points show uncorrected geodetic mass balance, while white points show geodetic mass balance corrected for internal ablation and additional melt from mapping dates to end of melt seasons Andreassen and others (2023). Glaciological glacier-wide SMB rate for Nigardsbreen over the same period shown as triangle (homogenized and calibrated record) and cross (homogenized only). Detached tongue of Brenndalsbreen (ID2301) not included due to scale (very negative median modelled SMB rate  $-3.70 \text{ m w.e. a}^{-1}$  with poor correspondence to geodetic rate  $-0.54 \text{ m w.e. a}^{-1}$ ).

946 Nigardsbreen. For each year we use available data over the period 1 July to 30 Sept, assuming that the ice  
947 surface is exposed over this period. In computing melt factors in mm w.e. from surface height difference  
948 we assume a density of ice of  $900 \text{ kg m}^{-3}$ . Estimated melt factors show large variability throughout the  
949 seasons (2.04–9.32 mm w.e.  $^{\circ}\text{C}^{-1}\text{d}^{-1}$ ). Our estimated value for  $MF_{ice, glob}$  (median  $\pm$  standard deviation)  
950 of  $5.11 \pm 0.51$  mm w.e.  $^{\circ}\text{C}^{-1}\text{d}^{-1}$  is a decent, although slightly lower, estimate than the median estimated  
951 melt factor for ice from the sonic ranger measurements in 2021 (6.14 mm w.e.  $^{\circ}\text{C}^{-1}\text{d}^{-1}$ ; 82 values) and  
952 2022 (5.28 mm w.e.  $^{\circ}\text{C}^{-1}\text{d}^{-1}$ ; 62 values).

953 We compare modelled accumulation from 1 October 2020 to 18 April 2021 using seNorge\_2018 with no  
954 temperature or precipitation correction ( $P_{corr}=1$ ,  $T_{corr}=0$   $^{\circ}\text{C}$ ; Fig. C4a) and modelled accumulation using  
955 the calibrated model (Fig. C4b) to snow radar measurements collected over the period 11–18 April 2021  
956 (personal communication from K. Melvold at NVE, March 2024). Snow radar point data was converted to  
957 the 1 km seNorge\_2018 grid with the point-to-raster function in ArcGIS Pro and the value in a given grid  
958 cell was taken as the average of all points in the cell. Measured snow depth in m was converted to m w.e.  
959 using snow density of  $404 \text{ kgm}^{-3}$  (measured for 5.5 m snow at 1791 m a.s.l. on Nigardsbreen on 14 April  
960 2021; Kjølmoen and others (2022)), giving a mean snow depth of 1.96 m w.e. Accumulation in 2020/21 is  
961 underestimated by around 23% when using raw (without correction) temperature and precipitation from  
962 seNorge\_2018 (Fig. C4a). The calibrated model gives lower discrepancy between modelled and measured  
963 snow depth (around 5%; Fig. C4b), but with slightly negative discrepancies in the south-central part of  
964 the ice cap and a tendency towards positive biases in the north and on north-eastern margins. However,  
965 magnitudes of  $P_{corr,j}$  agree relatively well with the magnitude of underestimation of accumulation using  
966 uncorrected seNorge\_2018.

## 967 APPENDIX D - ADDITIONAL FIGURES

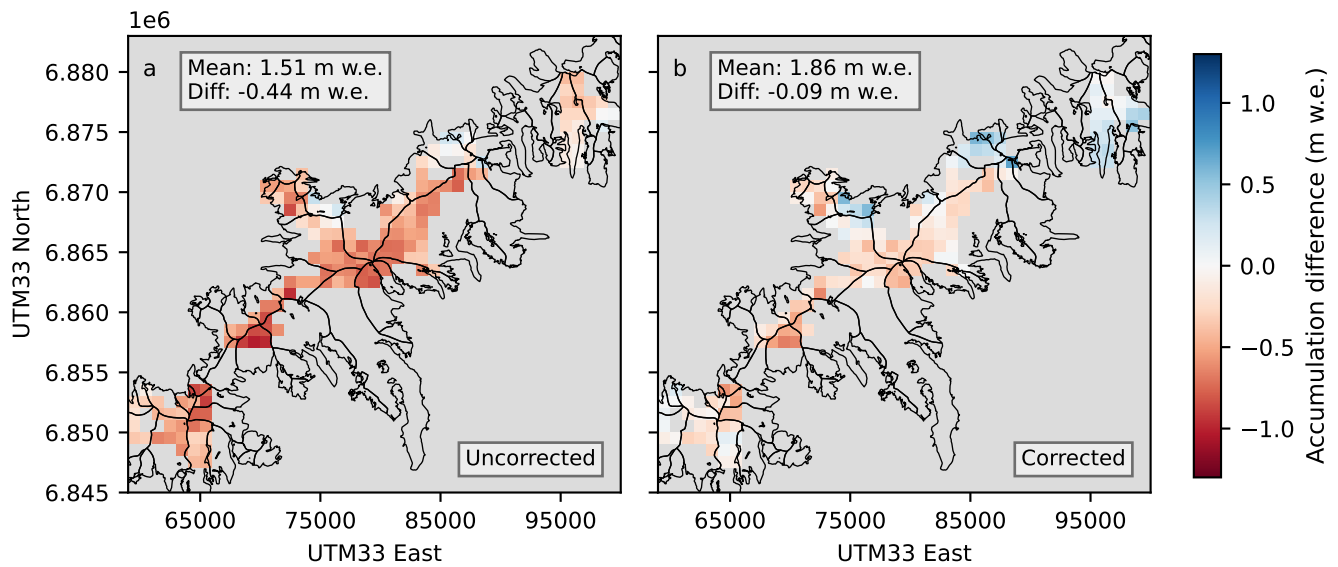


**Fig. C4.** Difference between modelled snow accumulation from 1 October 2020 to 18 April 2021 using seNorge\_2018 and estimated accumulation over parts of Jostedalsglacier using snow radar measurements from 11–18 April 2021 (a) without and (b) with spatial correction. Measured snow depth converted to m w.e. using snow density of  $404 \text{ kg m}^{-3}$  measured on 14 April 2021 (Kjøllmoen and others, 2022).

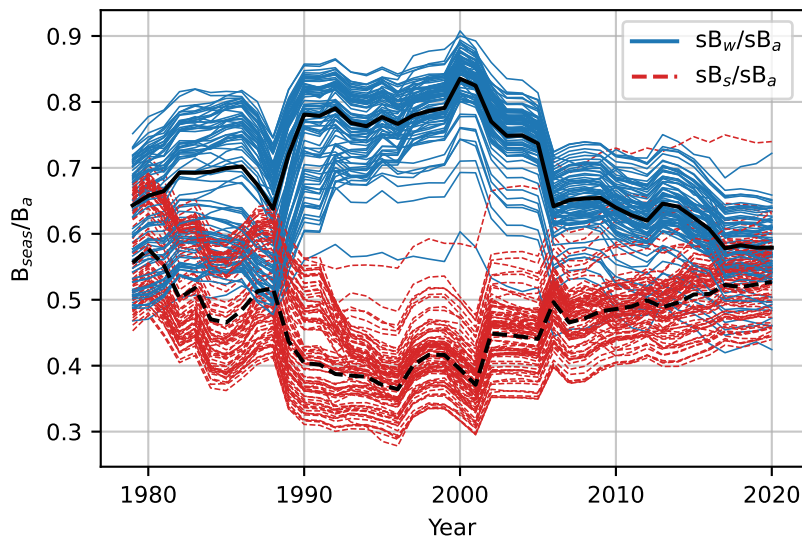


**Fig. D1.** Ratio of the standard deviation in winter surface mass balance (SMB) to annual SMB ( $sB_w/sB_a$ , solid blue lines) and summer SMB to annual SMB ( $sB_s/sB_a$ , dashed red lines) over 20-year rolling windows for each glacier of Jostedalsglacier ice cap. Jostedalsglacier as a whole is shown in bold black lines.